Neural Network-Assisted Hybrid Model Based Message Passing for Parametric Holographic MIMO Near Field Channel Estimation

Zhengdao Yuan, Yabo Guo, Dawei Gao, Qinghua Guo, *Senior Member, IEEE*, Zhongyong Wang, Chongwen Huang, Ming Jin, *Senior Member, IEEE* and Kai-Kit Wong, *Fellow, IEEE*

***Abstract*—Holographic multiple-input and multiple-output (HMIMO) is a promising technology with the potential to achieve high energy and spectral efficiencies, enhance system capacity and diversity, etc. In this work, we address the challenge of HMIMO near field (NF) channel estimation, which is complicated by the intricate model introduced by the dyadic Green's function. Despite its complexity, the channel model is governed by a limited set of parameters. This makes parametric channel estimation highly attractive, offering substantial performance enhancements and enabling the extraction of valuable sensing parameters, such as user locations, which are particularly beneficial in mobile networks. However, the relationship between these parameters and channel gains is nonlinear and compounded by integration, making the estimation a formidable task. To tackle this problem, we propose a novel neural network (NN) assisted hybrid method. With the assistance of NNs, we first develop a novel hybrid channel model with a significantly simplified expression compared to the original one, thereby enabling parametric channel estimation. Using the readily available training data derived from the original channel model, the NNs in the hybrid channel model can be effectively trained offline. Then, building upon this hybrid channel model, we formulate the parametric channel estimation problem with a probabilistic framework and design a factor graph representation for Bayesian estimation. Leveraging the factor graph representation and unitary approximate message passing (UAMP), we develop an effective message passing-based Bayesian channel estimation algorithm. Extensive simulations demonstrate the superior performance of the proposed method.**

***Index Terms*—Holographic MIMO, near field, Green's function, channel estimation, neural networks, message passing.**

I. Introduction

HOLOGRAPHIC multiple-input multiple-output (HMIMO) fulfills the deployment of extremely large and near spatial continuous surfaces within a compact space, harnessing the potential of electromagnetic (EM) channels. Recognized as a key enabling technology in future wireless communications, particularly in light of its potential integration into 6G networks, HMIMO holds substantial benefits in achieving high spectral and energy efficiencies, improves the system capacity and diversity, enhances massive connectivity, etc [1]–[8]

Recently, there has been a notable surge in research on HMIMO, leading to a multitude of investigations into its diverse applications in communication systems. Assuming perfect channel state information (CSI), studies such as those in [1] and [8] have delved into beamforming designs employing HMIMO for wireless communications. Research efforts like those in [3] and [4] have concentrated on tailored precoding designs for HMIMO systems, while others, such as those in [9] and [10], have addressed the holographic positioning problem. Additionally, integrated holographic sensing and communications have been explored in works such as [5] and [11]. Moreover, wireless power transfer has been extended to HMIMO systems [6]. Further exploration into wavenumber-division multiplexing within line-of-sight HMIMO communications has been undertaken in [7]. To leverage the full potential of HMIMO, efficient acquisition of accurate CSI is indispensable.

Some channel estimation methods have been proposed for HMIMO communications. In [12], considering both non-isotropic scattering and directive antennas, a channel model containing angle information for HMIMO was developed, and a novel channel estimation scheme was proposed, which exploits the rank deficiency induced by the array geometry and does not require exact channel statistics. With proper approximations to the channel covariance matrix, the work in [13] designed a low-complexity scheme to perform HMIMO channel estimation, which can achieve the same performance as the optimal minimum mean square error (MMSE) estimator. The work in [14] proposed a self-supervised machine learning channel estimation algorithm, which is designed to operate under more relaxed prior information. The work in [15] proposed decomposition and compressed deconstruction-based variational Bayesian inference

The work of Z. Yuan was supported by Science and Technology Research Project of Henan Province (252102210228). The work of D. Gao was supported by National Natural Science Foundation of China (62301394). The work of C. Huang was supported by the China National Key R and D Program under Grant 2021YFA1000500 and 2023YFB2904804, National Natural Science Foundation of China under Grant 62331023 and 62394292, Zhejiang Provincial Science and Technology Plan Project under Grant 2024C01033. (Corresponding authors: Qinghua Guo and Zhongyong Wang)

Z. Yuan is with the Artificial Intelligence Technology Engineering Research Center, Henan Open University, Zhengzhou 450002, China. He was with the School of Electrical, Computer and Telecommunications Engineering, University of Wollongong, Wollongong, NSW 2522, Australia (e-mail: yuan_zhengdao@foxmail.com).

Y. Guo and Z. Wang are with the School of Information Engineering, Zhengzhou University, Zhengzhou 450002, China. Y. Guo is also with the School of Electrical, Computer and Telecommunications Engineering, University of Wollongong, Wollongong, NSW 2522, Australia (e-mail: ieybguo@163.com, zywangzzu@gmail.com).

D. Gao is with the Hangzhou Institute of Technology, Xidian University, Hangzhou 311200, China. He was with with the School of Electrical, Computer and Telecommunications Engineering, University of Wollongong, NSW 2522, Australia (e-mail: gaodawei@xidian.edu.cn).

Q. Guo is with the School of Electrical, Computer and Telecommunications Engineering, University of Wollongong, Wollongong, NSW 2522, Australia (e-mail: qguo@uow.edu.au).

C. Huang is with College of Information Science and Electronic Engineering, Zhejiang University, Hangzhou 310027, China, and Zhejiang Provincial Key Laboratory of Multi-Modal Communication Networks and Intelligent Information Processing, Hangzhou 310027, China. (E-mail: chongwenhuang@zju.edu.cn).

M. Jin is with the Faculty of Electrical Engineering and Computer Science, Ningbo University, Ningbo 315211, China (e-mail: jinming@nbu.edu.cn)

K. K. Wong is affiliated with the Department of Electronic and Electrical Engineering, University College London, Torrington Place, WC1E 7JE, United Kingdom and he is also affiliated with Yonsei Frontier Lab, Yonsei University, Seoul, Korea (e-mail: kai-kit.wong@ucl.ac.uk).

to estimate azimuth and elevation angles, distance parameters, and sparse channels. In [16], leveraging the specific structure of the radiated beams generated by the continuous surface, a method based on a parametric physical channel model was proposed to estimate the line-of-sight dominated HMIMO channels in millimeter or THz bands. The aforementioned channel estimation methods are based on some simplified channel models with far-field assumption, which either break down at the near-field (NF) region or cannot capture the full-polarized information of EM fields [17], [18]. However, due to the large aperture of HMIMO surface and the use of high frequency band, which lead to a large Rayleigh distance, there is a need to consider HMIMO communications in NF. A low-complexity Bayes-optimal channel estimator operating in unknown EM environments was proposed in [19] for HMIMO systems, which has no requirements on priors or supervision, and relies on a statistical channel model. Model-driven deep learning methods have also been explored for HMIMO or extremely large MIMO channel estimation [20], [21]. HMIMIO channel estimation in the wavenumber domain has also been investigated [22], [23]. All of these methods are based on simplified channel models. However, to accurately characterize NF HMIMO channels, the use of the dyadic Green's function is necessitated, leading to intractable integration and nonlinearity in the channel model [4], [24]. To the best of our knowledge, the estimation of HMIMO NF channels characterized by dyadic Green's function has not been well addressed in the literature.

Despite the complexity of the channel model introduced by the dyadic Green's function, it is governed by a limited set of parameters. Compared to direct channel estimation methods that directly estimate a huge number of channel coefficients, parametric channel estimation is expected to achieve substantial performance enhancement. In addition, parametric channel estimation enables the extraction of valuable parameters, such as user locations, facilitating sensing in the networks. However, the relationship between the parameters and channel coefficients in HMIMO exhibits a convoluted nonlinearity compounded by integration, rendering parametric channel estimation a formidable task. To tackle this challenge, we propose a novel neural network (NN)-assisted hybrid approach. With the assistance of NNs, we first develop a novel hybrid HMIMO channel model, featuring a significantly simplified expression compared to the original one. This hybrid channel model enables parametric channel estimation. Using readily available training data derived from the original channel model, the NNs in the hybrid channel model can be effectively trained, which can be carried out offline. Subsequently, building upon this hybrid channel model, we formulate the parametric channel estimation problem in a probabilistic form for Bayesian estimation. With a factor graph representation of the parametric channel estimation problem and leveraging the unitary approximate message passing (UAMP) [25]–[27], an effective message passing-based Bayesian channel estimation algorithm is developed. Extensive simulation results are provided to demonstrate the superior performance of the proposed method. The main contributions of this work are summarized as follows:

- To the best of our knowledge, this is the first work on parametric channel estimation of HMIMO NF channels that are characterized using the Dyadic Green's function.
- Considering that HMIMO NF channels are governed by a small set of parameters, we estimate the parameters and subsequently reconstruct the channels, rather than directly estimating a large number of channel coefficients. This parametric approach leads to superior performance as the number of variables to be estimated is drastically reduced, and it also facilitates the sensing function in the system.
- To deal with the intractable dyadic Green's function based channel model, we propose an NN-assisted hybrid channel model, which can be well-trained offline. The NN-assisted hybrid channel model plays a crucial role in designing a practical HMIMO channel estimation algorithm.
- Building on the hybrid channel model, we formulate the parametric channel estimation problem into a probabilistic form and develop an effective message passing-based Bayesian channel estimation algorithm, leveraging UAMP.
- Extensive simulation results demonstrate the superior performance of the proposed method.
- Although this work focuses on HMIMO NF channel estimation, the hybrid model approach can be used to tackle a generic signal estimation problem involving a system transfer function, which is intractable using conventional approaches.

The remainder of this paper is organized as follows. In Section II, we introduce the signal model and formulate the HMIMO NF channel estimation problem. In Section III, a new hybrid channel model is proposed. Then the channel estimation problem is reformulated, and a factor graph representation is developed. Leveraging UAMP and the graph representation, a message passing algorithm is developed in Section IV. In Section V, we extend the discussion to HMIMO systems with the more practical hybrid analog-digital structure. Numerical results are provided in Section VI, followed by conclusions in Section VII.

Notations: Boldface lower-case and upper-case letters denote vectors and matrices, respectively. A Gaussian distribution of $\boldsymbol{x}$ with mean $\hat{\boldsymbol{x}}$ and covariance matrix $\boldsymbol{V}$ is represented by $\mathcal{CN}(\boldsymbol{x};\hat{\boldsymbol{x}},\boldsymbol{V})$. The relation $f(x) = cg(x)$ for some positive constant c is written as $f(x) \propto g(x)$, and $diag(\boldsymbol{a})$ returns a diagonal matrix with $\boldsymbol{a}$ on its diagonal. We use $\boldsymbol{A}\cdot\boldsymbol{B}$ and $\boldsymbol{A}\cdot/\boldsymbol{B}$ to denote the element-wise product and division between $\boldsymbol{A}$ and $\boldsymbol{B}$, respectively. The notation $|\boldsymbol{A}|^{\cdot 2}$ denotes an element-wise magnitude squared operation for $\boldsymbol{A}$, and $||\boldsymbol{A}||$ is the Frobenius norm of $\boldsymbol{A}$. We use $\mathbf{1}$, $\mathbf{0}$ and $\boldsymbol{I}$ to denote an all-one matrix, all-zero matrix and identity matrix with a proper size, respectively. The notation $x \sim \mathrm{U}[a,b]$ indicates that x has a uniform distribution over a and b.

II. Channel Model and Problem Formulation for HMIMO NF Channel Estimation

In this section, we introduce the dyadic Green's function based HMIMO channel model and the formulation of conventional channel estimation.

A. Channel Model Using the Dyadic Green's Function

We consider an HMIMO communication system shown in Fig. 1, where the receiver (base station) and transmitter (user) are equipped with holographic surfaces, comprising $M = M_{row} \times M_{col}$ and $N = N_{row} \times N_{col}$ patch antennas, respectively. Each patch can transmit or receive signals in three

polarizations [4]. Each transmit patch has a size of $\Delta_x^t \times \Delta_y^t$, and each receive path has a size of $\Delta_x^r \times \Delta_y^r$, where $\Delta_x^r, \Delta_y^r, \Delta_x^t$ and Δ_y^t denote the horizontal and vertical dimensions of receive and transmit patches. As shown in Fig. 1, we number the transmit and receive patches row by row. Assume that the receive surface lays in the xy plane and the center of the first receive patch is located at the origin of the coordinate system. The transmit surface is in parallel with the receive surface and the coordinate of the first transmit patch is denoted as $\boldsymbol{r}_1^t = (x_1^t, y_1^t, z_1^t)$. Denote the m-th receive patch and the n-th transmit patch as S_m^r and S_n^t, respectively. The coordinate vectors of the m-th receive and the n-th transmit patch centers are $\boldsymbol{r}_m^r = [x_m^r, y_m^r, z_m^r]^T$ and $\boldsymbol{r}_n^t = [x_n^t, y_n^t, z_n^t]^T$, respectively. Then the coordinates of the patch centers have the following relationship

$$\begin{aligned} &x_m^r = (c_m^r - 1)\Delta_x^r, \quad y_m^r = (l_m^r - 1)\Delta_y^r, \quad z_m^r = 0, \\ &x_n^t = x_1^t + (c_n^t - 1)\Delta_x^t, y_n^t = y_1^t + (l_n^t - 1)\Delta_y^t, z_n^t = z_1^t \end{aligned} \tag{1}$$

where $c_m^r = \text{mod}(m, M_{col})$, $l_m^r = \text{ceil}(m/M_{col})$, $c_n^t = \text{mod}(n, N_{col})$, $l_n^t = \text{ceil}(n/N_{col})$, $\text{mod}(\cdot)$ denotes the modulo operation and $\text{ceil}(\cdot)$ returns an smallest integer that is greater than or equal to the number in the parentheses.

We use $\boldsymbol{J}(\boldsymbol{r}^t)$ to denote the current generated at location $\boldsymbol{r}^t$ in the transmit surface S, then the radiated electric field $\boldsymbol{E}(\boldsymbol{r}^r)$ at the location $\boldsymbol{r}^r$ in the half free-space is given by the dyadic Green's function theorem as [4], [28]

$$\boldsymbol{E}(\boldsymbol{r}^r) = i\omega\mu \int_S \boldsymbol{G}(\boldsymbol{r}^t, \boldsymbol{r}^r)\boldsymbol{J}(\boldsymbol{r}^t)\mathrm{d}s, \tag{2}$$

where ω is permittivity, μ is permeability, and $\boldsymbol{G}(\boldsymbol{r}^t, \boldsymbol{r}^r)$ is dyadic Green's function [4], [24], [29], [30]

$$\boldsymbol{G}(\boldsymbol{r}^t, \boldsymbol{r}^r) = g(\boldsymbol{r}^t, \boldsymbol{r}^r)\left[c_1(r)\boldsymbol{I}_3 + c_2(r)\vec{\boldsymbol{r}}\vec{\boldsymbol{r}}^{\mathrm{T}}\right], \tag{3}$$

where

$$c_1(r) = 1 + \frac{i}{k_0 r} - \frac{1}{k_0^2 r^2}, \quad c_2(r) = \frac{3}{k_0^2 r^2} - \frac{3i}{k_0 r} - 1,$$

the unit vector $\vec{\boldsymbol{r}} = (\boldsymbol{r}^t - \boldsymbol{r}^r)/||\boldsymbol{r}^t - \boldsymbol{r}^r||$ denotes the direction between the source point and observation point, the scalar $r = ||\boldsymbol{r}^t - \boldsymbol{r}^r||$ denotes their distance, $\boldsymbol{I}_3$ denotes an identity matrix, $k_0 = 2\pi/\lambda$ is the wave number with λ being the wavelength, and the scalar Green's function $g(\boldsymbol{r}^t, \boldsymbol{r}^r)$ is given as

$$g(\boldsymbol{r}^t, \boldsymbol{r}^r) = \frac{\exp(ik_0||\boldsymbol{r}^t - \boldsymbol{r}^r||)}{4\pi||\boldsymbol{r}^t - \boldsymbol{r}^r||}. \tag{4}$$

Now we consider a single transmit patch S_n^t and a single receive patch S_m^r, and assume that the current distribution over the transmit patch is constant and there is no non-line-of-sight propagation [4]. Then the wireless channel with polarization between the n-th transmit patch and the m-th receive patch can be expressed as

$$\begin{aligned} \bar{\boldsymbol{H}}_{mn} = i\omega\mu \int_{x_m^r - \frac{\Delta_x^r}{2}}^{x_m^r + \frac{\Delta_x^r}{2}} \int_{y_m^r - \frac{\Delta_y^r}{2}}^{y_m^r + \frac{\Delta_y^r}{2}} \int_{x_n^t - \frac{\Delta_x^t}{2}}^{x_n^t + \frac{\Delta_x^t}{2}} \int_{y_n^t - \frac{\Delta_y^t}{2}}^{y_n^t + \frac{\Delta_y^t}{2}} \\ \boldsymbol{G}(\boldsymbol{r}^t, \boldsymbol{r}^r)\mathrm{d}y^t\mathrm{d}x^t\mathrm{d}y^r\mathrm{d}x^r. \end{aligned} \tag{5}$$

We note that $\bar{\boldsymbol{H}}_{mn}$ is a matrix with size 3×3, i.e.,

$$\bar{\boldsymbol{H}}_{mn} = \begin{bmatrix} h_{mn}^{xx} & h_{mn}^{xy} & h_{mn}^{xz} \\ h_{mn}^{xy} & h_{mn}^{yy} & h_{mn}^{yz} \\ h_{mn}^{xz} & h_{mn}^{yz} & h_{mn}^{zz} \end{bmatrix}, \tag{6}$$

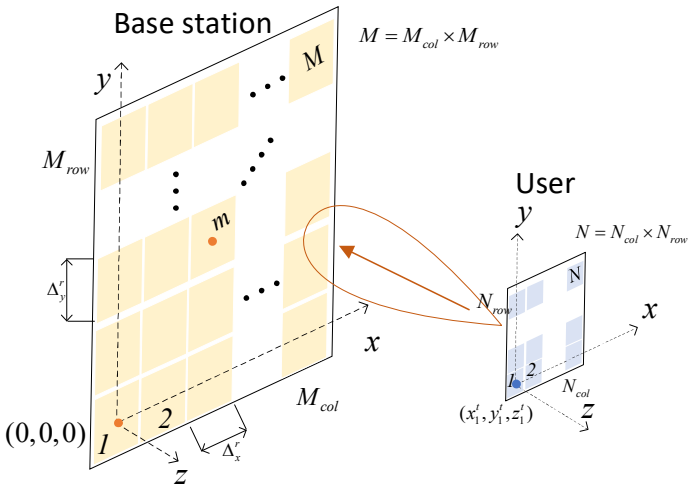

Fig. 1: Illustration of antenna patches and their coordinates.

where $h_{mn}^{\kappa}, \kappa \in \{xx, xy, xz, yy, yz, zz\}$ denotes the channel component corresponding to various transmit and receive polarization combinations. Considering all transmit and receive patches, we have the following channel matrix

$$\tilde{\boldsymbol{H}} \triangleq \begin{bmatrix} \bar{\boldsymbol{H}}_{11} & \cdots & \bar{\boldsymbol{H}}_{1N} \\ \vdots & \ddots & \vdots \\ \bar{\boldsymbol{H}}_{M1} & \cdots & \bar{\boldsymbol{H}}_{MN} \end{bmatrix} \in \mathbb{C}^{3M \times 3N}. \tag{7}$$

We can rearrange the elements in the matrix according to their polarization combinations, leading to a block matrix

$$\tilde{\boldsymbol{H}} = \begin{bmatrix} \tilde{\boldsymbol{H}}_{xx} & \tilde{\boldsymbol{H}}_{xy} & \tilde{\boldsymbol{H}}_{xz} \\ \tilde{\boldsymbol{H}}_{xy} & \tilde{\boldsymbol{H}}_{yy} & \tilde{\boldsymbol{H}}_{yz} \\ \tilde{\boldsymbol{H}}_{xz} & \tilde{\boldsymbol{H}}_{yz} & \tilde{\boldsymbol{H}}_{zz} \end{bmatrix}.$$

where $\tilde{\boldsymbol{H}}_{\kappa} \in \mathbb{C}^{M \times N}$ denotes the polarized channel matrix with $\kappa \in \{xx, xy, xz, yy, yz, zz\}$.

B. Problem Formulation for Channel Estimation

We start with the fully digital system, where each patch is connected to a RF chain. The more practical hybrid analog-digital architecture will be discussed in Section V of this paper.

Arranging L consecutive received signal vectors in a matrix $\tilde{\boldsymbol{Y}}$, we have

$$\tilde{\boldsymbol{Y}} = \tilde{\boldsymbol{H}}\tilde{\boldsymbol{S}} + \tilde{\boldsymbol{W}}, \tag{8}$$

where $\tilde{\boldsymbol{Y}} \triangleq [\tilde{\boldsymbol{Y}}_x^T, \tilde{\boldsymbol{Y}}_y^T, \tilde{\boldsymbol{Y}}_z^T]^T \in \mathbb{C}^{3M \times L}$ with the subscripts denoting the polarization direction and $\tilde{\boldsymbol{Y}}_x, \tilde{\boldsymbol{Y}}_y, \tilde{\boldsymbol{Y}}_z \in \mathbb{C}^{M \times L}$. $\tilde{\boldsymbol{S}} \triangleq [\tilde{\boldsymbol{S}}_x^T, \tilde{\boldsymbol{S}}_y^T, \tilde{\boldsymbol{S}}_z^T]^T \in \mathbb{C}^{3N \times L}$ with $\tilde{\boldsymbol{S}}_x, \tilde{\boldsymbol{S}}_y, \tilde{\boldsymbol{S}}_z \in \mathbb{C}^{N \times L}$ denoting the pilot matrices in x, y and z polarization, $\tilde{\boldsymbol{W}} \triangleq [\tilde{\boldsymbol{W}}_x^T, \tilde{\boldsymbol{W}}_y^T, \tilde{\boldsymbol{W}}_z^T]^T \in \mathbb{C}^{3M \times L}$ represents the zero mean complex additive white Gaussian noise (AWGN) with precision γ (i.e., variance γ^{-1}).

To facilitate channel estimation, we can rearrange the signal model into the following form

$$\begin{aligned}\boldsymbol{Y} &= \begin{bmatrix} \tilde{\boldsymbol{S}}_x^{\mathrm{T}} & 0 & 0 & \tilde{\boldsymbol{S}}_y^{\mathrm{T}} & \tilde{\boldsymbol{S}}_z^{\mathrm{T}} & 0 \\ 0 & \tilde{\boldsymbol{S}}_y^{\mathrm{T}} & 0 & \tilde{\boldsymbol{S}}_x^{\mathrm{T}} & 0 & \tilde{\boldsymbol{S}}_z^{\mathrm{T}} \\ 0 & 0 & \tilde{\boldsymbol{S}}_z^{\mathrm{T}} & 0 & \tilde{\boldsymbol{S}}_x^{\mathrm{T}} & \tilde{\boldsymbol{S}}_y^{\mathrm{T}} \end{bmatrix} \begin{bmatrix} \boldsymbol{H}_{xx} \\ \boldsymbol{H}_{yy} \\ \boldsymbol{H}_{zz} \\ \boldsymbol{H}_{xy} \\ \boldsymbol{H}_{xz} \\ \boldsymbol{H}_{yz} \end{bmatrix} + \bar{\boldsymbol{W}} \\ &\triangleq \boldsymbol{S}\boldsymbol{H} + \bar{\boldsymbol{W}}, \end{aligned} \tag{9}$$

where $\boldsymbol{Y} \triangleq [\tilde{\boldsymbol{Y}}_x, \tilde{\boldsymbol{Y}}_y, \tilde{\boldsymbol{Y}}_z]^T \in \mathbb{C}^{3L\times M}$, $\boldsymbol{S} \in \mathbb{C}^{3L\times 6N}$, $\boldsymbol{H} \in \mathbb{C}^{6N\times M}$ and $\boldsymbol{H}_\kappa = \tilde{\boldsymbol{H}}_\kappa^T$ with $\kappa \in \{xx, xy, xz, yy, yz, zz\}$, which is given as

$$\boldsymbol{H}_\kappa \triangleq \begin{bmatrix} h_{11}^\kappa & \cdots & h_{1M}^\kappa \\ \vdots & \ddots & \vdots \\ h_{N1}^\kappa & \cdots & h_{NM}^\kappa \end{bmatrix}. \tag{10}$$

In addition, $\bar{\boldsymbol{W}} \triangleq [\tilde{\boldsymbol{W}}_x, \tilde{\boldsymbol{W}}_y, \tilde{\boldsymbol{W}}_z]^T \in \mathbb{C}^{3L\times M}$ denotes the white Gaussian noise.

Our aim is to estimate the channel matrix $\boldsymbol{H}$ based on the pilot signals $\boldsymbol{S}$ and received signal $\boldsymbol{Y}$. Regarding this, we have the following remarks:

- One straightforward method is to estimate the channel coefficients directly e.g., using the least squares (LS) method. It is noted the number of the variables to be estimated is $6MN$, which lead to high pilot overhead to achieve satisfactory performance and high computational complexity due to the involved large matrix inversion.
- According to (5), the channel coefficients are parameterized by $\boldsymbol{r}^r$ and $\boldsymbol{r}^t$ (noting that $\boldsymbol{r}^r$ is known). This motivates us to perform parametric channel estimation to drastically reduce the number of variables to be estimated, thereby achieving significantly enhanced performance. That is, we first estimate $\boldsymbol{r}^t$, based on which the channel matrix can be reconstructed. This is the strategy of parametric channel estimation used in this work.
- It can be seen from (5) that there is a complex relationship between $\bar{\boldsymbol{H}}_{mn}$ and $\boldsymbol{r}^t$, leading to challenges in parametric channel estimation. In [4], with some approximations, an approximate analytical expression for the HMIMO channel is obtained, i.e.,

$$\begin{aligned}\bar{\boldsymbol{H}}_{mn} \approx i\omega\mu\Delta^t\Delta^r \frac{\exp(ik_0 r_{mn})}{4\pi r_{mn}} \times \\ \operatorname{sinc}\frac{k_0(x_m^r - x_n^t)\Delta_x^t}{2r_{mn}} \operatorname{sinc}\frac{k_0(y_m^r - y_n^t)\Delta_y^t}{2r_{mn}} \boldsymbol{C}_{mn}, \end{aligned} \tag{11}$$

  where $\Delta^t = \Delta_x^t\Delta_y^t$ and $\Delta^r = \Delta_x^r\Delta_y^r$ represent the area of transmitter and receiver patch, respectively, $r_{mn} = ||\boldsymbol{r}_n^t - \boldsymbol{r}_m^r||$ and $\boldsymbol{C}_{mn} = c_1(r_{mn})\boldsymbol{I}_3 + c_2(r_{mn})\vec{\boldsymbol{r}}\vec{\boldsymbol{r}}^T$ with $c_1(r_{mn})$ and $c_2(r_{mn})$ are given in (3) by replacing $\boldsymbol{r}^t$ and $\boldsymbol{r}^r$ with the $\boldsymbol{r}_n^t$ and $\boldsymbol{r}_m^r$, respectively. However, the approximate channel model still has a complex expression with nonlinear operations, making parametric channel estimation challenging. Moreover, it can also lead to significant mismatch with the true channel due to the approximations.
- In this work, we propose a novel NN-assisted hybrid channel model to characterize the nonlinear relationship between $\boldsymbol{H}$ and $\boldsymbol{r}^t$, which has a much simpler expression, enabling efficient parametric channel estimation.

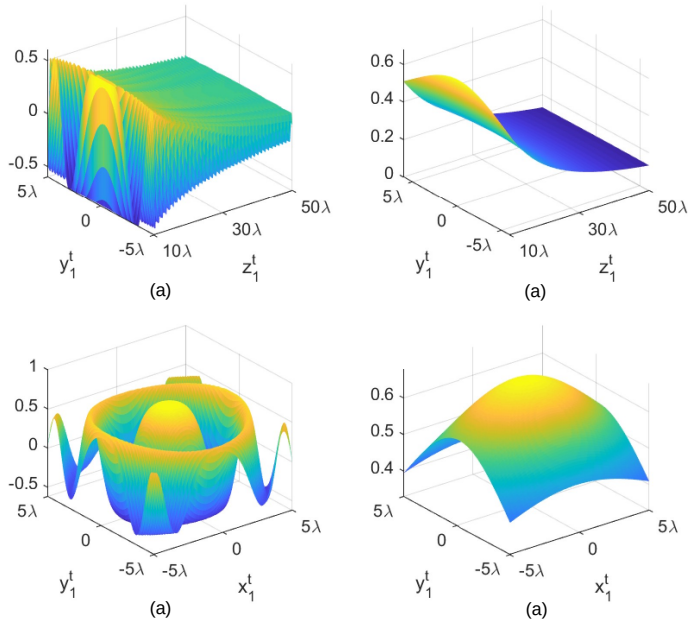

Fig. 2: (a) and (c): the real part of h_{11}^{xx}; (b) and (d): the real part of $h_{11}^{xx}/\exp(ik_0 r_{11})$.

III. NN-Assisted Hybrid Channel Model and Parametric Channel Estimation

In this section, we propose an NN-assisted hybrid channel model and the training of the involved NN, which enables parametric channel estimation.

A. NN-Assisted Hybrid Channel Model

According to (5), the channel components between the m-th receive patch and the n-th transmit patch, which is denoted as h_{mn}^κ, is parameterized by $\{x_n^t, y_n^t, z_n^t\}$ (noting that the coordinates of the receive patch centers are known). An idea is to develop an NN model with the parameters as input modes to replace (5). However, this is not the best way. Take the channel component h_{11}^κ, which corresponds to the 1st transmit patch and the 1st receive patch, as an example. In Fig. 2 (a) and (c), we show the real part of h_{11}^{xx} respectively with a fixed x_1^t and a fixed z_1^t. We can see that they are rather complex and change abruptly, which makes it necessary to use NNs with high expressive capability, leading to the requirement of a large number of NN parameters. This will result in high complexity in training and parametric channel estimation channel estimation.

The decayed periodicity-like pattern exhibited in Fig. 2 (a) and (c) motivates us to examine the variation of the quantity

$$\tilde{h}_{11}^{xx} = h_{11}^{xx}(x_1^t, y_1^t, z_1^t)/\exp(ik_0 r_{11}), \tag{12}$$

where $r_{11} = ||\boldsymbol{r}_1^t - \boldsymbol{r}_1^r||$. Its real part is shown in Fig. 2 (b) and (d), where we can see that it changes much slowly. Hence, it can be potentially characterized by a much simpler NN. In particular, we use an NN with a single hidden layer as shown in Fig. 3 in this work.

It is not hard to show that the channel components between the m-th receive patch and the n-th transmit patch actually depends on their relative position. Then we define $x_{mn} = x_n^t - x_m^r, y_{mn} = y_n^t - y_m^r, z_{mn} = z_n^t - z_m^r$ $\boldsymbol{r}_{mn} = [x_{nm}, y_{nm}, z_{nm}]^T$ and $r_{mn} = ||\boldsymbol{r}_{mn}||$. Hence, we have

$$\tilde{h}_{mn}^\kappa = h_{mn}^\kappa(x_{mn}, y_{mn}, z_{mn})/\exp(ik_0 r_{mn}), \tag{13}$$

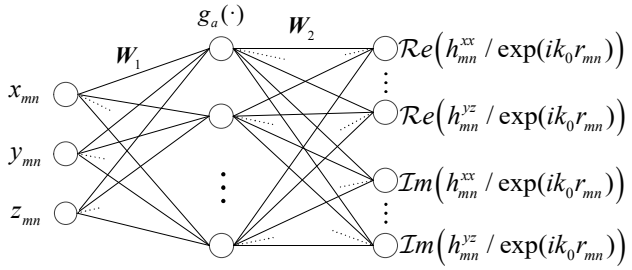

Fig. 3: Architecture of the neural network.

where $\kappa \in \{xx, xy, xz, yy, yz, zz\}$. This allows us to use a single NN to characterize the channel components between any transmit patch and receive patch, facilitating the NN training and Bayesian inference algorithm design later.

As shown in Fig. 3, we use a real-valued NN, where we separate the real and imaginary parts of the relevant variables. Its inputs are the relative coordinates x_{mn}, y_{mn} and z_{mn}, and the outputs are $\{Re\{\tilde{h}_{mn}^{\kappa}\}, Im\{\tilde{h}_{mn}^{\kappa}\}, \kappa \in \{xx, xy, xz, yy, yz, zz\}\}$. According to Fig. 3, the output of the neural network can be expressed as

$$\begin{aligned} &\mathcal{NN}(x_{mn}, y_{mn}, z_{mn}) \\ &= \boldsymbol{W}_2^{\mathrm{T}} g_a(\boldsymbol{w}_1^x x_{mn} + \boldsymbol{w}_1^y y_{mn} + \boldsymbol{w}_1^z z_{mn} + \boldsymbol{b}_1) + \boldsymbol{b}_2, \\ &\triangleq \boldsymbol{\xi}_{mn} \in \mathbb{R}^{12\times 1} \end{aligned} \tag{14}$$

where $\boldsymbol{W}_1 = [\boldsymbol{w}_1^x, \boldsymbol{w}_1^y, \boldsymbol{w}_1^z] \in \mathbb{R}^{N_h \times 3}$ is the input layer weight matrix with $\boldsymbol{w}_1^x, \boldsymbol{w}_1^y, \boldsymbol{w}_1^z \in \mathbb{R}^{N_h \times 1}$, $\boldsymbol{W}_2 = [\boldsymbol{w}_{2,1}, \cdots, \boldsymbol{w}_{2,12}] \in \mathbb{R}^{N_h \times 12}$ is the output layer weight matrix with $\{\boldsymbol{w}_{2,1}, \cdots, \boldsymbol{w}_{2,12}\} \in \mathbb{R}^{N_h \times 1}$, output $\boldsymbol{\xi}_{mn} = \mathcal{NN}(x_{mn}, y_{mn}, z_{mn}) \in \mathbb{R}^{12\times 1}$, N_h is the number of neurons in the hidden layer, $\boldsymbol{b}_1 \in \mathbb{R}^{N_h \times 1}$ and $\boldsymbol{b}_2 \in \mathbb{R}^{12\times 1}$ are bias vectors in the hidden layer and output layer respectively. The activation function in the hidden layer $g_a(\cdot) = tansig(\cdot)$ and a linear activation function is used at the output layer.

We put two outputs in Fig. 3, which correspond to the real and imaginary parts of $\tilde{h}_{mn}^{\kappa}$ together and denote it as $\varphi^{\kappa}(x_{mn}, y_{mn}, z_{mn})$. For example, for the xx polarization, we combine the first and the 7-th outputs of the neural network into a complex number, i.e., $\varphi^{xx}(x_{mn}, y_{mn}, z_{mn}) = \boldsymbol{\xi}_{mn}(1) + i\boldsymbol{\xi}_{mn}(7)$. Then we have the following hybrid channel model

$$h_{mn}^{\kappa} \approx \varphi^{\kappa}(x_{mn}, y_{mn}, z_{mn}) \exp(ik_0 r_{mn}), \tag{15}$$

where $\varphi^{\kappa}(x_{mn}, y_{mn}, z_{mn})$ is the output of the NN. We can see that, with the aid of NN, we convert the channel model with complex expression (5) to (15), which has a closed form with much simpler expression. It is noted that all the operations involved in (14) and (15) are linear, except the nonlinear operations due to the activation function $g_a(\cdot)$ in the NN and multiplication operation in (15). The hybrid channel model enables tractable Bayesian inference for parametric channel estimation detailed in Section IV.

According to (1), the relative coordinates can be expressed as functions of $\{x_1^t, y_1^t, z_1^t\}$ or $\{x_n^t, y_n^t, z_n^t\}, \forall n$, i.e.,

$$\begin{aligned} x_{mn} &= x_n^t - x_m^r = x_1^t + (c_n^t - 1)\Delta_x^t - x_m^r = x_1^t + \Delta_{mn}^x \\ y_{mn} &= y_n^t - y_m^r = y_1^t + (l_n^t - 1)\Delta_y^t - y_m^r = y_1^t + \Delta_{mn}^y \\ z_{mn} &= z_n^t = z_1^t. \end{aligned} \tag{16}$$

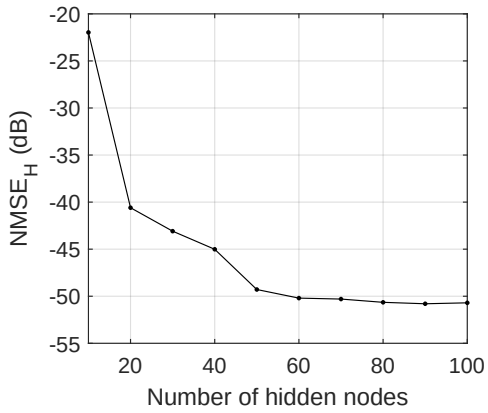

Fig. 4: NMSE of channel modeling versus the number of hidden nodes.

It is noted that the coordinates of the receive patches $\{x_m^r, y_m^r\}$ are known. This means that any channel component h_{nm}^{κ} can be expressed as a function of the coordinate of the first transmit patch $\{x_1^t, y_1^t, z_1^t\}$, which will be estimated. With the estimated coordinate, the channel components can be obtained using (15). We define a new function $\phi_{mn}^{\kappa}(x_n^t, y_n^t, z_n^t)$, which is a shifted version of $\varphi^{\kappa}(x_{mn}, y_{mn}, z_{mn})$, i.e.,

$$\phi_{mn}^{\kappa}(x_n^t, y_n^t, z_n^t) = \varphi^{\kappa}(x_n^t - x_m^r, y_n^t - y_m^r, z_n^t), \tag{17}$$

which will be used later in the inference algorithm design.

B. Neural Network Training

The training of the NN can be easily implemented. This is because, with the original model (5), sufficient training samples can be easily generated using numerical methods. We note that the whole training process can be carried out offline. The NN is trained with the back propagation using the following loss function

$$\mathrm{L} = \frac{1}{MN} \sum_{m,n,\kappa} ||\varphi_{mn}^{\kappa}(x_{mn}, y_{mn}, z_{mn}) - \tilde{h}^{\kappa}(x_{mn}, y_{mn}, z_{mn})||^2$$

where $\tilde{h}^{\kappa}(x_{mn}, y_{mn}, z_{mn})$ are calculated using (5) and (13).

The number of hidden nodes has an impact on the accuracy of the NN model. Fig. 4 shows the normalized mean squared error (NMSE) of the constructed channel using the NN model with true transmitter locations versus the number of hidden nodes. We can see that the NMSE performance improves with the number of hidden nodes. When the number of hidden nodes is larger than 50, the NMSE reaches about -50dB and the performance improvement is marginal with the further increase in the number of hidden nodes. Hence, we choose the number of hidden nodes to be 50.

IV. Probabilistic Formulation, Factor Graph Representation and Message Passing Algorithm

In this section, with the NN-assisted hybrid channel model in Section III, we formulate the parametric channel estimation problem in a probabilistic form. We will compute the (approximate) marginals of transmitter coordinates and the HMIMO channel components, based on which their estimates can be obtained. It is worth noting that the estimates of the transmitter

coordinates and the HMIMO channel components admit the constraint due to the hybrid channel mode, so that accurate channel estimation can be achieved. With the probabilistic formulation in Section IV.A, we represent the problem in a factor graph in Section IV.B, and develop a message passing algorithm, which involves a forward process in Section IV. C and a backward process in Section IV.D. The complexity of the algorithm is also analyzed.

A. Probabilistic Formulation

We develop a Bayesian parametric channel estimation method, where UAMP, a variant of the AMP algorithm, is used to achieve low complexity while with high robustness. To facilitate the use of UAMP, we carry out a unitary transformation to (9) based on the singular value decomposition (SVD) $\boldsymbol{S}=\boldsymbol{U}\boldsymbol{\Lambda}\boldsymbol{V}$, i.e.,

$$\boldsymbol{R}=\boldsymbol{\Phi}\boldsymbol{H}+\boldsymbol{W}, \tag{18}$$

where $\boldsymbol{R}=\boldsymbol{U}^H\boldsymbol{Y}\in\mathbb{C}^{3L\times M}$, $\boldsymbol{\Phi}=\boldsymbol{U}^H\boldsymbol{S}\in\mathbb{C}^{3L\times 6N}$, and $\boldsymbol{W}=\boldsymbol{U}^H\bar{\boldsymbol{W}}\in\mathbb{C}^{3L\times M}$ still represents zero-mean white Gaussian noise with the same variance because $\boldsymbol{U}^H$ is a unitary matrix.

The conditional joint probability density function of the unknown variables given the observation matrix $\boldsymbol{R}$ can be factorized as

$$\begin{aligned}
&p(\boldsymbol{H},\gamma,\{x_n^t,y_n^t,z_n^t,n\neq 1\},x_1^t,y_1^t,z_1^t|\boldsymbol{R})\\
&\propto p(\boldsymbol{R}|\boldsymbol{H},\gamma)\prod\nolimits_{n\neq 1,m}p(\boldsymbol{h}_{mn}|x_n^t,y_n^t,z_n^t)p(x_n^t|x_1^t)\\
&\quad\times p(y_n|y_1^t)p(z_n|z_1^t)p(x_1^t)p(y_1^t)p(z_1^t)p(\gamma)\\
&\triangleq f_{\boldsymbol{R}}(\boldsymbol{R},\boldsymbol{H},\gamma)\prod\nolimits_{n\neq 1,m}f_{h_{mn}}(\boldsymbol{h}_{mn},x_n^t,y_n^t,z_n^t)f_{x_n^t}(x_n^t,x_1^t)\\
&\times f_{y_n^t}(y_n^t,y_1^t)f_{z_n^t}(z_n^t,z_1^t)f_{x_1^t}(x_1^t)f_{y_1^t}(y_1^t)f_{z_1^t}(z_1^t)f_\gamma(\gamma),
\end{aligned} \tag{19}$$

where γ is the precision of the noise and it is treated as a random variable with an improper prior $p(\gamma)\propto 1/\gamma$, the function $f_{\boldsymbol{R}}(\boldsymbol{R},\boldsymbol{H},\gamma)=\mathcal{CN}(\boldsymbol{R};\boldsymbol{\Phi}\boldsymbol{H},\gamma^{-1}\boldsymbol{I})$, the function $f_{h_{mn}}(\boldsymbol{h}_{mn},x_n^t,y_n^t,z_n^t)$ can be further decomposed into

$$f_{h_{mn}}(\boldsymbol{h}_{mn},x_n^t,y_n^t,z_n^t)=\prod_\kappa f_{h_{mn}}^\kappa(h_{mn}^\kappa,x_n^t,y_n^t,z_n^t),$$

with $\boldsymbol{h}_{mn}=[h_{mn}^{xx},...,h_{mn}^{zz}]^T\in\mathbb{C}^{6\times 1}$ and $f_{h_{mn}}^\kappa(x_n^t,y_n^t,z_n^t)=\delta(h_{mn}^\kappa-\phi_{mn}^\kappa\exp(ik_0r_{mn}))$ (the arguments x_n^t,y_n^t,z_n^t of the function ϕ_{mn}^κ are omitted for notation simplicity), the function $f_{x_n^t}(x_n^t,x_1^t)=\delta\left(x_n^t-(x_1^t+(c_n^t-1)\Delta_x^t)\right)$ according to (16), $f_{x_1}(x_1^t)$ represents the prior of x_1^t, which is selected to be a non-informative one, e.g., a Gaussian distribution with an infinite variance. Other functions $f_{y_n^t}(y_n^t,y_1^t)$, $f_{z_n^t}(z_n^t,z_1^t)$, $f_{y_1^t}(y_1^t)$ and $f_{z_1^t}(z_1^t)$ have similar definitions as $f_{x_n^t}$ and f_{x_1}, as shown in Table I. Our aim is to compute the (approximate) marginals of the coordinates x_1^t,y_1^t,z_1^t and the channel components, based on which their estimates can be obtained.

B. Factor Graph Representation

To facilitate the factor graph representation of the factorization in (19), we list the involved notations in Table II, showing the correspondence between the factor labels and the underlying distributions they represent, and the specific functional form assumed by each factor. In this section, we investigate how to efficiently solve the formulated channel estimation problem with message passing-based Bayesian inference.

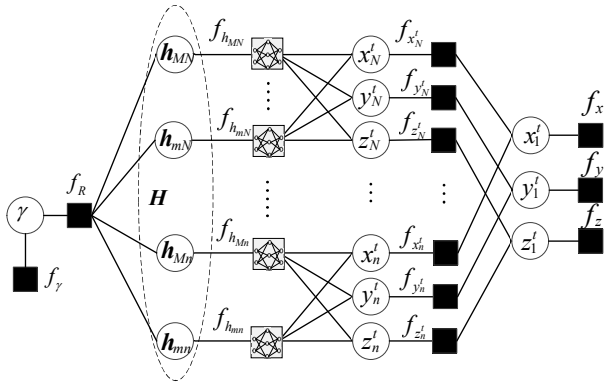

Fig. 5: Factor graph representation of (19)

.

The factor graph representation for the factorization in (19) is visualized in Fig. 5, where squares and circles represent function nodes and variable nodes, respectively. It is noted that the message passing algorithm is performed in an iterative manner, where each iteration involves a forward message passing process and backward message passing process in the graph shown in Fig. 5. We use $m_{A\to B}(\mu)$ to denote a message passed from node A to node B, which is a function of μ. For Gaussian messages, the arrows above its mean and variance indicate the message passing direction. In addition, we use $b(\mu)$ to denote the belief of a variable μ. Note that, if a forward computation requires backward messages, the relevant messages in the previous iteration is used by default. Next we elaborate on the forward and backward message computations. To facilitate derivations, a scalar representation of the part of the graph is shown in Fig. 6 to show the detailed relationship between the hybrid function nodes and variable nodes.

C. Forward Message Passing

From the factorization (19), the likelihood function $p(\boldsymbol{R}|\boldsymbol{H},\gamma)$ is a linear mixed model and can be handled using UAMP [25]–[27]. With UAMP, we can compute the mean and variances about the entries in matrix $\boldsymbol{H}$ in the following. Following UAMP, we first compute matrices $\boldsymbol{V}_P$ and $\boldsymbol{P}$ as

$$\begin{aligned}
\boldsymbol{V}_P &= |\boldsymbol{\Phi}|^{.2}\boldsymbol{V}_H,\\
\boldsymbol{P} &= \boldsymbol{\Phi}\hat{\boldsymbol{H}}-\boldsymbol{V}_P\cdot\boldsymbol{S}_H,
\end{aligned}$$

where $\hat{\boldsymbol{H}}$ is the mean matrix of $\boldsymbol{H}$ and $\boldsymbol{V}_H$ contains the variances of the corresponding elements in $\boldsymbol{H}$, which will be

TABLE I: Local functions and distributions in (19)

Factor	Distribution	Function
$f_{\boldsymbol{R}}$	$p(\boldsymbol{R}\|\boldsymbol{H},\gamma)$	$\mathcal{CN}(\boldsymbol{R};\boldsymbol{\Phi}\boldsymbol{H},\gamma^{-1}\boldsymbol{I})$
$f_{h_{mn}}^\kappa$	$p(\boldsymbol{h}_{mn}\|x_n^t,y_n^t,z_n^t)$	$\prod_\kappa\delta(h_{mn}^\kappa-\phi_{mn}^\kappa\exp(ik_0r_{mn}))$
$f_{x_n^t}$	$p(x_n\|x_1^t)$	$\delta\left(x_n^t-(x_1^t+(c_n^t-1)\Delta_x^t)\right)$
$f_{y_n^t}$	$p(y_n\|y_1^t)$	$\delta\left(y_n^t-(y_1^t+(l_n^t-1)\Delta_y^t)\right)$
$f_{z_n^t}$	$p(z_n\|z_1^t)$	$\delta\left(z_n^t-z_1^t\right)$
$f_{x_1^t}$,$f_{y_1^t}$,$f_{z_1^t}$	$p(x_1^t),p(y_1^t),p(z_1^t)$	non-informative
f_γ	$p(\gamma)$	$1/\gamma$

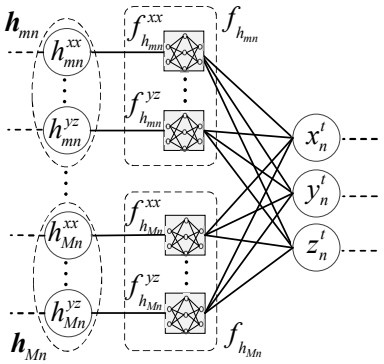

Fig. 6: Scalar factor graph representation related to the hybrid local function nodes.

updated in (50) based on the posterior distribution $b(\boldsymbol{H})$, and $\boldsymbol{S}_H$ will be updated (64). The precision of the noise γ can be estimated as

$$\hat{\gamma} = \frac{3ML}{||\boldsymbol{R}-\boldsymbol{Z}||^2 + \boldsymbol{V}_Z}, \tag{20}$$

where the auxiliary matrices $\boldsymbol{V}_Z$ and $\boldsymbol{Z}$ can be computed as

$$\boldsymbol{V}_Z = \boldsymbol{V}_P./(\hat{\gamma}\boldsymbol{V}_P + 1), \tag{21}$$
$$\boldsymbol{Z}_E = (\hat{\gamma}\boldsymbol{R} + \boldsymbol{P}./\boldsymbol{V}_P)\cdot \boldsymbol{V}_Z. \tag{22}$$

Then, we update intermediate matrices $\boldsymbol{V}_{S_H}$ and $\boldsymbol{S}_H$ as

$$\begin{aligned}\boldsymbol{V}_{S_H} &= 1./(\boldsymbol{V}_P + \hat{\gamma}^{-1}),\\ \boldsymbol{S}_H &= \boldsymbol{V}_{S_H}\cdot(\boldsymbol{R}-\boldsymbol{P}),\end{aligned} \tag{23}$$

and obtain matrices $\boldsymbol{V}_{Q_H}$ and $\boldsymbol{Q}_H$ as

$$\boldsymbol{V}_{Q_H} = 1./(|\boldsymbol{\Phi}^H|^{.2}\boldsymbol{V}_{S_H}), \tag{24}$$
$$\boldsymbol{Q}_H = \hat{\boldsymbol{H}} + \boldsymbol{V}_{Q_H}\cdot(\boldsymbol{\Phi}^H\boldsymbol{S}_H). \tag{25}$$

Matrices $\boldsymbol{Q}_H$ and $\boldsymbol{V}_{Q_H}$ can be respectively represented as

$$\boldsymbol{Q}_H = \begin{bmatrix}\boldsymbol{Q}_{H_{xx}}\\ \vdots \\ \boldsymbol{Q}_{H_{yz}}\end{bmatrix}, \quad \boldsymbol{V}_{Q_H} = \begin{bmatrix}\boldsymbol{V}_{Q_H^{xx}}\\ \vdots \\ \boldsymbol{V}_{Q_H^{yz}}\end{bmatrix}. \tag{26}$$

where $\boldsymbol{Q}_{H_\kappa} \in \mathbb{C}^{N\times M}$ and $\boldsymbol{V}_{Q_H^\kappa} \in \mathbb{R}^{N\times M}, \kappa \in \{xx, ..., zz\}$ with their (n,m)-th element denoted as q_{mn}^κ and $\nu_{q_{mn}^\kappa}$, respectively. Here q_{mn}^κ and $\nu_{q_{mn}^\kappa}, \forall\kappa$, represent the mean and variance of message $m_{h_{mn}^\kappa \to f_{h_{mn}^\kappa}}(h_{mn}^\kappa)$, i.e.,

$$m_{h_{mn}^\kappa \to f_{h_{mn}^\kappa}}(h_{mn}^\kappa) = \mathcal{CN}(h_{mn}^\kappa; q_{mn}^\kappa, \nu_{q_{mn}^\kappa}). \tag{27}$$

From the factor graph, we can see that the message updates for x_1^t, y_1^t and z_1^t are similar. So in the following, we take x_1^t as an example for the derivation of the message update rules. It can be seen from (15) that the local function node $f_{h_{mn}}^\kappa$ still involves nonlinear operations, leading to intractable messages. To overcome the problem, we propose using Taylor expansion to dynamically linearize the node $f_{h_{mn}}^\kappa$. To this end, we approximate h_{mn}^κ as

$$\begin{aligned}
&h_{mn}^\kappa(x_n^t, y_n^t, z_n^t)\\
&\approx \underbrace{h_{mn}^\kappa(\hat{x}_n^t, \hat{y}_n^t, \hat{z}_n^t)}_{\hat{h}_{mn}^\kappa} + \underbrace{h_{mn}^{\kappa,x'}(\hat{x}_n^t, \hat{y}_n^t, \hat{z}_n^t)}_{\hat{h}_{mn}^{\kappa,x'}}(x_n^t - \hat{x}_n^t)\\
&\quad + \underbrace{h_{mn}^{\kappa,y'}(\hat{x}_n^t, \hat{y}_n^t, \hat{z}_n^t)}_{\hat{h}_{mn}^{\kappa,y'}}(y_n^t - \hat{y}_n^t) + \underbrace{h_{mn}^{\kappa,y'}(\hat{x}_n^t, \hat{y}_n^t, \hat{z}_n^t)}_{\hat{h}_{mn}^{\kappa,z'}}(z_n^t - \hat{z}_n^t)\\
&= \underbrace{\hat{h}_{mn}^\kappa - \hat{h}_{mn}^{\kappa,x'}\hat{x}_n^t - \hat{h}_{mn}^{\kappa,y'}\hat{y}_n^t - \hat{h}_{mn}^{\kappa,z'}\hat{z}_n^t}_{\xi_{mn}^\kappa}\\
&\quad + x_n^t\hat{h}_{mn}^{\kappa,x'} + y_n^t\hat{h}_{mn}^{\kappa,y'} + z_n^t\hat{h}_{mn}^{\kappa,z'}\\
&= \xi_{mn}^\kappa + x_n^t\hat{h}_{mn}^{\kappa,x'} + y_n^t\hat{h}_{mn}^{\kappa,y'} + z_n^t\hat{h}_{mn}^{\kappa,z'}.
\end{aligned} \tag{28}$$

where $h_{mn}^{\kappa,x'}$ represents the partial derivative of h_{mn}^κ with respect to x_n^t, and similarly, $h_{mn}^{\kappa,y'}$ and $h_{mn}^{\kappa,z'}$ are the partial derivatives with respect to y_n^t and z_n^t, respectively. The partial derivative of $h_{mn}^{\kappa,x'}$ can be obtained as

$$h_{mn}^{\kappa,x'} = \frac{\partial h_{mn}^\kappa}{\partial x_n^t} = \left(\frac{\partial \phi_{mn}^\kappa}{\partial x_n^t} + \phi_{mn}^\kappa ik_0\frac{\partial r_{mn}}{\partial x_n^t}\right)\exp(ik_0 r_{mn}). \tag{29}$$

The derivatives of ϕ_{mn}^κ can be get by

$$\begin{aligned}\frac{\partial \phi_{mn}^\kappa}{\partial x_n^t} &= ((\boldsymbol{w}_{2,\kappa_1} + \boldsymbol{w}_{2,\kappa_2})\cdot \boldsymbol{w}_1^x)^{\mathrm{T}}\\ &\quad \times g_a'(x_n^t\boldsymbol{w}_1^x + y_n^t\boldsymbol{w}_1^y + z_n^t\boldsymbol{w}_1^z + \boldsymbol{b}_1),\end{aligned}$$

where the values of indices κ_1 and κ_2 depend on the polarization parameter $\kappa \in \{xx, ..., zz\}$. For example, if $\kappa = xx$, we have $\kappa_1 = 1$ and $\kappa_2 = 7$. The derivative of $g_a(\cdot)$ is $g_a'(\cdot) = 1 - g_a^2(\cdot)$.

According to (28), we can rewrite the function $f_{h_{mn}^\kappa}$ as

$$f_{h_{mn}^\kappa} = \delta\left(h_{mn}^\kappa - (\xi_{mn}^\kappa + x_n^t\hat{h}_{mn}^{\kappa,x'} + y_n^t\hat{h}_{mn}^{\kappa,y'} + z_n^t\hat{h}_{mn}^{\kappa,z'})\right). \tag{30}$$

Assume that the backward messages $m_{y_n^t \to f_{h_{mn}^\kappa}^\kappa}(y_n^t)$ and $m_{z_n^t \to f_{h_{mn}^\kappa}^\kappa}(z_n^t)$ are available, which turn out to be Gaussian (please refer to a similar message $m_{x_n^t \to f_{h_{mn}^\kappa}^\kappa}(x_n^t)$ in (44) that is derived later) and can be expressed as

$$m_{y_n^t \to f_{h_{mn}^\kappa}^\kappa}(y_n^t) = \mathcal{CN}\left(y_n^t; \overleftarrow{y}_{mn}^\kappa, \overleftarrow{\nu}_{y_{mn}^\kappa}\right), \tag{31}$$
$$m_{z_n^t \to f_{h_{mn}^\kappa}^\kappa}(z_n^t) = \mathcal{CN}\left(z_n^t; \overleftarrow{z}_{mn}^\kappa \overleftarrow{\nu}_{z_{mn}^\kappa}\right). \tag{32}$$

Then the message from $f_{h_{mn}^\kappa}$ to x_n^t can be computed as

$$\begin{aligned}m_{f_{h_{mn}^\kappa} \to x_n^t}(x_n^t) &= \int f_{h_{mn}^\kappa} m_{y_n^t \to f_{h_{mn}^\kappa}^\kappa}(y_n^t) m_{z_n^t \to f_{h_{mn}^\kappa}^\kappa}(z_n^t)\\ &\quad \times m_{h_{mn}^\kappa \to f_{h_{mn}^\kappa}}(h_{mn}^\kappa)\mathrm{d}y_n^t\mathrm{d}z_n^t\mathrm{d}h_{mn}^\kappa\\ &= \mathcal{CN}\left(x_n^t; \vec{x}_{mn}^\kappa, \vec{\nu}_{x_{mn}}^\kappa\right),\end{aligned} \tag{33}$$

where

$$\vec{x}_{mn}^\kappa = \frac{q_{mn}^\kappa - \xi_{mn}^\kappa - \overleftarrow{y}_{mn}^\kappa\hat{h}_{mn}^{\kappa y'} - \overleftarrow{z}_{mn}^\kappa\hat{h}_{mn}^{\kappa z'}}{\hat{h}_{mn}^{\kappa x'}}, \tag{34}$$

$$\vec{\nu}_{x_{mn}}^\kappa = \frac{\nu_{q_{mn}^\kappa} + \overleftarrow{\nu}_{y_{mn}^\kappa}|\hat{h}_{mn}^{\kappa y'}|^2 + \overleftarrow{\nu}_{z_{mn}^\kappa}|\hat{h}_{mn}^{\kappa z'}|^2}{|\hat{h}_{mn}^{\kappa x'}|^2}. \tag{35}$$

Then, the forward message from x_n^t to $f_{x_n^t}$ can be expressed as

$$\begin{aligned}m_{x_n^t \to f_{x_n^t}}(x_n^t) &= \prod_{m,\kappa} m_{f_{h_{mn}^\kappa} \to x_n^t}(x_n^t)\\ &= \mathcal{CN}(x_n^t, \vec{x}_n^t, \vec{\nu}_{x_n^t}),\end{aligned} \tag{36}$$

where $\vec{\nu}_{x_n^t} = 1/(\sum_{m,\kappa} 1/\vec{\nu}^{\kappa}_{x_{mn}})$ and $\vec{x}_n^t = \vec{\nu}_{x_n^t} \sum_{m,\kappa} \vec{x}^{\kappa}_{mn}/\vec{\nu}^{\kappa}_{x_{mn}}$. So the message $m_{f_{x_n^t}\to x_1^t}(x_1^t)$ can be computed as

$$\begin{aligned} m_{f_{x_n^t}\to x_1^t}(x_1^t) &= \int f_{x_n^t} m_{x_n^t\to f_{x_n^t}}(x_n^t)\mathrm{d}x_n^t \\ &= \mathcal{CN}\left(x_1^t; \vec{x}_n, \vec{\nu}_{x_n}\right), \end{aligned} \tag{37}$$

where $\vec{x}_n = \vec{x}_n^t - w_n^x$ and $\vec{\nu}_{x_n} = \vec{\nu}_{x_n^t}$. Then, the belief of x_1^t can be expressed as

$$b(x_1^t) = \frac{\prod_n m_{f_{x_n^t}\to x_1^t}(x_1^t)}{\int \prod_n m_{f_{x_n^t}(x)\to x_1^t}(x_1^t)\mathrm{d}x_1^t} = \mathcal{N}(x_1^t, \hat{x}_1^t, \nu_{x_1^t}), \tag{38}$$

where $\nu_{x_1^t} = 1/(\sum_n 1/\vec{\nu}_{x_n})$ and $\hat{x}_1^t = \nu_{x_1^t}\sum_n \vec{x}_n/\vec{\nu}_{x_n}$.

D. Backward Message Passing

With belief propagation, the backward message $m_{x_1^t\to f_{x_n^t}}(x_1^t)$ can be computed as

$$m_{x_1^t\to f_{x_n^t}}(x_1^t) = \frac{b(x_1^t)}{m_{f_{x_n^t}\to x_1^t}(x_1^t)} = \mathcal{N}(x_1^t; \overleftarrow{x}_n, \overleftarrow{\nu}_{x_n}), \tag{39}$$

where $\overleftarrow{\nu}_{x_n} = 1/(1/\nu_{x_1^t} - 1/\vec{\nu}_{x_1^t})$ and $\overleftarrow{x}_n = \overleftarrow{\nu}_{x_n}(\hat{x}_1^t/\nu_{x_1^t} - \vec{x}_n/\vec{\nu}_{x_n})$. Then the backward message $m_{f_{x_n^t}\to x_n^t}(x_n^t)$ can be updated by

$$\begin{aligned} m_{f_{x_n^t}\to x_n^t}(x_n^t) &= \int f_{x_n^t} m_{x\to f_{u_{xn}}}(x_n^t)\mathrm{d}x_n^t \\ &= \mathcal{N}(x_n^t; \overleftarrow{x}_n^t, \overleftarrow{\nu}_{x_n^t}), \end{aligned} \tag{40}$$

where $\overleftarrow{x}_n^t = \overleftarrow{x}_n + w_n^x$ and $\overleftarrow{\nu}_{x_n^t} = \overleftarrow{\nu}_{x_n}$. So the belief of x_n^t can be computed as

$$\begin{aligned} b(x_n^t) &= \frac{m_{f_{x_n^t}\to x_n^t}(x_n^t) m_{x_n^t\to f_{x_n^t}}(x_n^t)}{\int m_{f_{x_n^t}\to x_n^t}(x_n^t) m_{x_n^t\to f_{x_n^t}}(x_n^t)\mathrm{d}x_n^t} \\ &= \mathcal{N}(x_n^t; \hat{x}_n^t, \nu_{x_n^t}), \end{aligned} \tag{41}$$

with mean $\hat{x}_n^t$ and variance $\nu_{x_n^t}$ given as

$$\nu_{x_n^t} = 1/(1/\overleftarrow{\nu}_{x_n^t} + 1/\vec{\nu}_{x_n^t}), \tag{42}$$

$$\hat{x}_n^t = \nu_{x_n^t}(\overleftarrow{x}_n^t/\overleftarrow{\nu}_{x_n^t} + \vec{x}_n^t/\vec{\nu}_{x_n^t}). \tag{43}$$

Based on $b(x_n^t)$, we have

$$\begin{aligned} m_{x_n^t\to f_{h^{\kappa}_{mn}}}(x_n^t) &= \frac{b(x_n^t)}{m_{f_{h^{\kappa}_{mn}}\to x_n^t}(x_n^t)} \\ &= \mathcal{N}(x_n^t; \overleftarrow{x}^{\kappa}_{mn}, \overleftarrow{\nu}^{\kappa}_{x_{mn}}), \end{aligned} \tag{44}$$

where mean $\overleftarrow{x}^{\kappa}_{mn}$ and variance $\overleftarrow{\nu}^{\kappa}_{x_{mn}}$ are given by

$$\overleftarrow{\nu}^{\kappa}_{x_{mn}} = 1/(1/\nu_{x_n^t} - 1/\vec{\nu}^{\kappa}_{x_{mn}}), \tag{45}$$

$$\overleftarrow{x}^{\kappa}_{mn} = \overleftarrow{\nu}^{\kappa}_{x_{mn}}(\hat{x}_n^t/\nu_{x_n^t} - \vec{x}^{\kappa}_{mn}/\vec{\nu}^{\kappa}_{x_{mn}}). \tag{46}$$

Then, we can update the message from $f^{\kappa}_{h_{mn}}$ to h^{κ}_{mn} by

$$\begin{aligned} m_{f_{h^{\kappa}_{mn}}\to h^{\kappa}_{mn}}(h^{\kappa}_{mn}) &= \int f_{h^{\kappa}_{mn}} m_{x_n^t\to f_{h^{\kappa}_{mn}}}(x_n^t) \\ &\times m_{y_n^t\to f_{h^{\kappa}_{mn}}}(y_n^t) m_{z_n^t\to f_{h^{\kappa}_{mn}}}(z_n^t)\mathrm{d}x_n^t\mathrm{d}y_n^t\mathrm{d}z_n^t \\ &= \mathcal{N}(h_{mn}; \overleftarrow{h}^{\kappa}_{mn}, \overleftarrow{\nu}^{\kappa}_{h_{mn}}), \end{aligned} \tag{47}$$

where

$$\overleftarrow{\nu}^{\kappa}_{h_{mn}} = \xi^{\kappa}_{mn} + \overleftarrow{x}^{\kappa}_{mn}\hat{h}^{\kappa x'}_{mn} + \overleftarrow{y}^{\kappa}_{mn}\hat{h}^{\kappa y'}_{mn} + \overleftarrow{z}^{\kappa}_{mn}\hat{h}^{\kappa z'}_{mn}, \tag{48}$$

$$\overleftarrow{h}^{\kappa}_{mn} = \overleftarrow{\nu}^{\kappa}_{x_{mn}}|\hat{h}^{\kappa x'}_{mn}|^2 + \overleftarrow{\nu}^{\kappa}_{y_{mn}}|\hat{h}^{\kappa y'}_{mn}|^2 + \overleftarrow{\nu}^{\kappa}_{z_{mn}}|\hat{h}^{\kappa z'}_{mn}|^2. \tag{49}$$

Then we can obtain the belief of channel component h^{κ}_{mn} as

$$\begin{aligned} b(h^{\kappa}_{mn}) &= m_{f_{h^{\kappa}_{mn}}\to h^{\kappa}_{mn}}(h^{\kappa}_{mn}) m_{h^{\kappa}_{mn}\to f_{h^{\kappa}_{mn}}}(h^{\kappa}_{mn}) \\ &= \mathcal{CN}(h^{\kappa}_{mn}; \hat{h}^{\kappa}_{mn}, \nu_{h^{\kappa}_{mn}}) \end{aligned} \tag{50}$$

where

$$\begin{aligned} \nu_{h^{\kappa}_{mn}} &= 1/(1/\overleftarrow{\nu}^{\kappa}_{h_{mn}} + 1/\nu_{q^{\kappa}_{mn}}) \\ \hat{h}^{\kappa}_{mn} &= \nu_{h^{\kappa}_{mn}}(\overleftarrow{h}^{\kappa}_{mn}/\overleftarrow{\nu}^{\kappa}_{h_{mn}} + q^{\kappa}_{mn}/\nu_{q^{\kappa}_{mn}}). \end{aligned} \tag{51}$$

We stack $\nu_{h^{\kappa}_{mn}}$ and $\hat{h}^{\kappa}_{mn}, \forall m, n, \kappa$ as matrices $\boldsymbol{V}_H$ and $\hat{\boldsymbol{H}}$. This is the end of backward message passing.

The message passing algorithm is summarized in Algorithm 1, which is called NNHMP (NN-assisted hybrid model based message passing). The iteration can be terminated when it reaches the preset maximum number of iterations or the difference between the estimates of two consecutive iterations is less than a threshold. We can see that the NNHMP algorithm includes three parts: UAMP part (Lines 1-7), the part related to the NN-assisted hybrid local function node (Line 9) and the part producing location estimation (Lines 9-19). The UAMP part is dominated by matrix multiplication with a complexity of $\mathcal{O}(MNL)$. In the part related to the NN node, in total MN channel elements are involved, and a multiplication of two matrices with dimensions $3 \times N_h$ and $N_h \times 12$ is performed, so the complexity is $\mathcal{O}(MNN_h^2)$, where N_h denotes the number of hidden nodes. In the remaining part, the highest complexity lies in the computation of message $m_{f_{h^{\kappa}_{nm}}\to x_n^t}(x_n^t), \forall n, \kappa$ in (37), whose complexity is $\mathcal{O}(MN)$.

Algorithm 1 NNHMP for Parametric Channel Estimation

Initialization: $\hat{\boldsymbol{H}} = \mathbf{0}_{6N\times M}$, $\boldsymbol{V}_H = \mathbf{1}_{6N\times M}$, $\boldsymbol{S}_H = \mathbf{0}_{3L\times M}$, $\kappa \in \{xx, xy, xz, yy, yz, zz\}$.

Repeat

1: $\boldsymbol{V}_P = |\boldsymbol{\Phi}|^{\cdot 2}\boldsymbol{V}_H$
2: $\boldsymbol{P} = \boldsymbol{\Phi}\hat{\boldsymbol{H}} - \boldsymbol{V}_P \cdot \boldsymbol{S}_H$
3: $\boldsymbol{V}_{S_H} = 1./(\boldsymbol{V}_P + \gamma^{-1})$
4: $\boldsymbol{S}_H = \boldsymbol{V}_{S_H} \cdot (\boldsymbol{R} - \boldsymbol{P})$
5: $\boldsymbol{V}_{Q_H} = 1./(|\boldsymbol{\Phi}^H|^{\cdot 2}\boldsymbol{V}_{S_H})$
6: $\boldsymbol{Q}_H = \hat{\boldsymbol{H}} + \boldsymbol{V}_{Q_H} \cdot (\boldsymbol{\Phi}^H \boldsymbol{S}_H)$
7: get γ by (20)
8: $\forall n, m, \kappa$: Compute $\hat{h}^{\kappa x'}_{mn}, \hat{h}^{\kappa y'}_{mn}, \hat{h}^{\kappa z'}_{mn}, \xi^{\kappa}_{mn}$ with (28)
9: $\forall n, m, \kappa$: Compute $m_{f^{\kappa}_{h_{mn}}\to x_n^t}$ with (33)
10: $\forall n$: Compute $m_{x_n^t\to f_{x_n^t}}$ with (36)
11: $\forall n$: Compute $m_{f_{x_n^t}\to x_1^t}$ with (37)
12: Compute belief $b(x_1^t)$ with (38)
13: $\forall n$: Compute $m_{f_{x_n^t}\to x_n^t}$ with (40)
14: $\forall n$: Compute $m_{x_1^t\to f_{x_n^t}}$ with (39)
15: $\forall n$: Compute belief $b(x_n^t)$ with (41)
16: $\forall n, m, \kappa$: get $m_{x_n^t\to f_{h^{\kappa}_{mn}}}$ with (44)
17: Compute $m_{y_n^t\to f_{h^{\kappa}_{mn}}}$ and $m_{z_n^t\to f_{h^{\kappa}_{mn}}}$ with the procedure similar to Lines 10-17
18: $\forall n, m, \kappa$: Compute $m_{f_{h^{\kappa}_{mn}}\to h^{\kappa}_{mn}}$ with (47)
19: $\forall n, m, \kappa$: get $b(h^{\kappa}_{mn}) = \mathcal{CN}(h^{\kappa}_{mn}; \hat{h}^{\kappa}_{mn}, \nu_{h^{\kappa}_{mn}})$ by (50)
20: Stack $\hat{h}^{\kappa}_{mn}, \nu_{h^{\kappa}_{mn}}, \forall n, m, \kappa$ into $\hat{\boldsymbol{H}}$ and $\boldsymbol{V}_H$

Until terminated

V. Channel Estimation with Hybrid Receiver

In the previous section, we assume a fully digital receiver, where each antenna patch is connected to an RF chain [12], [13].

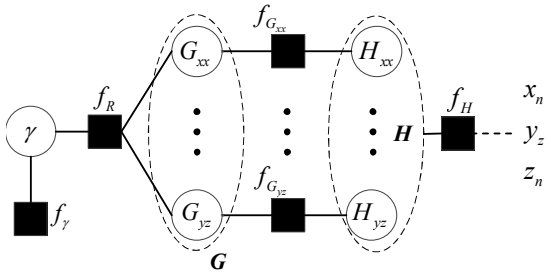

Fig. 7: Factor graph representation of (55).

In this section, we consider a more practical hybrid structure [19], [31], where the holographic surface is connected to P ($P < M$) RF chains. This leads to a $3P \times 3M$ matrix $\tilde{\boldsymbol{F}}$ in the signal model, i.e., the received signal can be expressed as

$$\tilde{\boldsymbol{Y}} = \tilde{\boldsymbol{F}}\tilde{\boldsymbol{H}}\tilde{\boldsymbol{S}} + \tilde{\boldsymbol{W}}, \tag{52}$$

where $\tilde{\boldsymbol{Y}} \triangleq [\tilde{\boldsymbol{Y}}_x^{\mathrm{T}}, \tilde{\boldsymbol{Y}}_y^{\mathrm{T}}, \tilde{\boldsymbol{Y}}_z^{\mathrm{T}}]^{\mathrm{T}} \in \mathbb{C}^{3P\times L}$ with $\tilde{\boldsymbol{Y}}_x, \tilde{\boldsymbol{Y}}_y$ and $\tilde{\boldsymbol{Y}}_z \in \mathbb{C}^{P\times L}$, and $\tilde{\boldsymbol{S}}$, $\tilde{\boldsymbol{H}}$ and $\tilde{\boldsymbol{W}}$ are the same as those in (8). To facilitate channel estimation, the model is rewritten as

$$\begin{aligned}\boldsymbol{Y} &= \boldsymbol{S}\begin{bmatrix}(\boldsymbol{F}\tilde{\boldsymbol{H}}_{xx})^{\mathrm{T}}\\ \vdots \\ (\boldsymbol{F}\tilde{\boldsymbol{H}}_{yz})^{\mathrm{T}}\end{bmatrix} + \boldsymbol{W} = \boldsymbol{S}\begin{bmatrix}\boldsymbol{G}_{xx}\\ \vdots \\ \boldsymbol{G}_{yz}\end{bmatrix} + \boldsymbol{W}\\ &\triangleq \boldsymbol{S}\boldsymbol{G} + \boldsymbol{W},\end{aligned} \tag{53}$$

where $\boldsymbol{Y} \triangleq [\tilde{\boldsymbol{Y}}_x, \tilde{\boldsymbol{Y}}_x, \tilde{\boldsymbol{Y}}_x]^{\mathrm{T}} \in \mathbb{C}^{3L\times P}$. Define $\boldsymbol{G} \triangleq [\boldsymbol{G}_{xx}^{\mathrm{T}}, \cdots, \boldsymbol{G}_{yz}^{\mathrm{T}}]^{\mathrm{T}} \in \mathbb{C}^{6N\times P}$ and

$$\boldsymbol{G}_\kappa^{\mathrm{T}} = \boldsymbol{F}\tilde{\boldsymbol{H}}_\kappa = \boldsymbol{F}\boldsymbol{H}_\kappa^{\mathrm{T}} \in \mathbb{C}^{P\times N}, \tag{54}$$

where $\boldsymbol{H}_\kappa$ has the same definition in (9). Comparing it with model (18), we can see that the difference lies in the likelihood function $p(\boldsymbol{R}|\boldsymbol{H}, \lambda)$, which can be expressed as

$$\begin{aligned}p(\boldsymbol{R}|\boldsymbol{G}, \boldsymbol{H}, \lambda) &= p(\boldsymbol{R}|\boldsymbol{G}, \gamma)\textstyle\prod_\kappa p(\boldsymbol{G}_\kappa|\boldsymbol{H}_\kappa)p(\gamma)\\ &= f_R(\boldsymbol{R}, \boldsymbol{G}, \gamma)\textstyle\prod_\kappa f_{G_\kappa}(\boldsymbol{G}_\kappa, \boldsymbol{H}_\kappa)p(\gamma)\end{aligned} \tag{55}$$

where $p(\boldsymbol{R}|\boldsymbol{G}, \gamma) = \mathcal{CN}(\boldsymbol{R}; \boldsymbol{\Phi}\boldsymbol{G}, \gamma^{-1}\boldsymbol{I})$ and $p(\boldsymbol{G}_\kappa|\boldsymbol{H}_\kappa) = \delta(\boldsymbol{G}_\kappa^{\mathrm{T}} - \boldsymbol{F}\boldsymbol{H}_\kappa^{\mathrm{T}})$ with $\boldsymbol{\Phi}$ and $\boldsymbol{R}$ defined in (19).

TABLE II: Local functions and distributions in (55)

Factor	Distribution	Function
$f_R(\boldsymbol{R}, \boldsymbol{G}, \gamma)$	$p(\boldsymbol{R}\|\boldsymbol{G}, \gamma)$	$\mathcal{CN}(\boldsymbol{R}; \boldsymbol{\Phi}\boldsymbol{G}, \gamma^{-1}\boldsymbol{I})$
$f_{G_\kappa}(\boldsymbol{G}_\kappa, \boldsymbol{H}_\kappa)$	$p(\boldsymbol{G}_\kappa\|\boldsymbol{H}_\kappa)$	$\delta(\boldsymbol{G}_\kappa^{\mathrm{T}} - \boldsymbol{F}\boldsymbol{H}_\kappa^{\mathrm{T}})$
f_γ	$p(\gamma)$	$1/\gamma$

Part of the graph representation in this case is shown in Fig.7, and the remaining part of the graph representation is the same as that in Fig.5. Hence, we focus on message passing in Fig.7 in this section. It can be seen from the factorization (55) that there are two successive linear mixing operations involved in the signal model, which are $f_{\boldsymbol{R}}(\boldsymbol{R}, \boldsymbol{G}, \gamma)$ and $f_{\boldsymbol{G}_\kappa}(\boldsymbol{G}_\kappa, \boldsymbol{H}_\kappa)$. To solve the problem, we propose using the cascade of two UAMP algorithms.

A. UAMP for $f_{\boldsymbol{R}}(\boldsymbol{R}, \boldsymbol{G}, \gamma)$

We can see from (55) that $p(\boldsymbol{R}|\boldsymbol{G}, \gamma)$ has essentially the same expression as $p(\boldsymbol{R}|\boldsymbol{H}, \gamma)$ in (19). Similar to (62)-(66), we have the following steps according to UAMP.

We first compute matrices $\boldsymbol{V}_{P_G}$ and $\boldsymbol{P}_G$ by

$$\begin{aligned}\boldsymbol{V}_{\boldsymbol{P}_G} &= |\boldsymbol{\Phi}|^{\cdot 2}\boldsymbol{V}_G,\\ \boldsymbol{P}_G &= \boldsymbol{\Phi}\hat{\boldsymbol{G}} - \boldsymbol{V}_{P_G}\cdot\boldsymbol{S}_G,\end{aligned}$$

where $\boldsymbol{\Phi} = \boldsymbol{\Lambda}_G\boldsymbol{V}_G$ and $[\boldsymbol{U}_G, \Lambda_G, \boldsymbol{V}_G] = \mathrm{SVD}(\boldsymbol{S})$.The estimate of the noise precision is updated as

$$\hat{\gamma} = \frac{3PL}{||\boldsymbol{R} - \boldsymbol{Z}_G||^2 + \boldsymbol{V}_{Z_G}}, \tag{56}$$

where

$$\begin{aligned}\boldsymbol{V}_{Z_G} &= 1./(\hat{\gamma} + 1./\boldsymbol{V}_{P_G}),\\ \boldsymbol{Z}_G &= \boldsymbol{V}_{Z_G}\cdot(\hat{\gamma}\boldsymbol{R} + \boldsymbol{P}_G./\boldsymbol{V}_{P_G}).\end{aligned}$$

Then the two intermediate matrices can be computed by

$$\begin{aligned}\boldsymbol{V}_{S_G} &= 1./(\boldsymbol{V}_{P_G} + \hat{\gamma}^{-1}),\\ \boldsymbol{S}_G &= \boldsymbol{V}_{S_G}\cdot(\boldsymbol{R} - \hat{\boldsymbol{P}}_G).\end{aligned}$$

After that we can get $\boldsymbol{V}_{Q_G}$ and $\boldsymbol{Q}_G$ as

$$\boldsymbol{V}_{Q_G} = 1./(|\boldsymbol{\Phi}^{\mathrm{H}}|^{\cdot 2}\boldsymbol{V}_{S_G}), \tag{57}$$

$$\boldsymbol{Q}_G = \hat{\boldsymbol{G}} + \boldsymbol{V}_{Q_G}\cdot(\boldsymbol{\Phi}^{\mathrm{H}}\boldsymbol{S}_G), \tag{58}$$

They can be represented using block matrices as

$$\boldsymbol{V}_{Q_G} = \begin{bmatrix}\boldsymbol{V}_{Q_G^{xx}}\\ \vdots \\ \boldsymbol{V}_{Q_G^{yz}}\end{bmatrix}, \quad \boldsymbol{Q}_G = \begin{bmatrix}\boldsymbol{Q}_{G_{xx}}\\ \vdots \\ \boldsymbol{Q}_{G_{yz}}\end{bmatrix}. \tag{59}$$

where $\boldsymbol{V}_{Q_G^\kappa} \in \mathbb{R}^{N\times P}$ and $\boldsymbol{Q}_{G_\kappa} \in \mathbb{C}^{N\times P}$ with their (n, m)-th element being $\vec{g}_{mn}^\kappa$ and $\vec{\nu}_{g_{mn}^\kappa}$. They provide the mean and variance of message $m_{g_{mn}^\kappa\to f_{g_{mn}^\kappa}}(g_{mn}^\kappa)$, i.e., $m_{g_{mn}^\kappa\to f_{g_{mn}^\kappa}}(g_{mn}^\kappa) = \mathcal{CN}(g_{mn}^\kappa; \vec{g}_{mn}^\kappa, \vec{\nu}_{g_{mn}^\kappa})$. Then the belief of g_{mn}^κ is $b(g_{mn}^\kappa) = \mathcal{CN}(g_{mn}^\kappa; \hat{g}_{mn}^\kappa, \nu_{g_{mn}^\kappa})$, where

$$\begin{aligned}\nu_{g_{mn}^\kappa} &= 1/(1/\vec{\nu}_{g_{mn}^\kappa} + 1/\nu_{p_{h_{mn}^\kappa}})\\ \hat{g}_{mn}^\kappa &= \nu_{g_{mn}^\kappa}(\vec{g}_{mn}^\kappa/\vec{\nu}_{g_{mn}^\kappa} + p_{h_{mn}^\kappa}/\nu_{p_{h_{mn}^\kappa}})\end{aligned} \tag{60}$$

with $p_{h_{mn}^\kappa}$ and $\nu_{p_{h_{mn}^\kappa}}$ being the (n, m)-th member of $\boldsymbol{P}_{H_\kappa}$ and $\boldsymbol{V}_{P_{H_\kappa}}$, and they are updated in (63) and (62). Next, we stack $\hat{g}_{mn}^\kappa$ and $\nu_{g_{mn}^\kappa}, \forall m, n, \kappa$ into matrices $\hat{\boldsymbol{G}}$ and $\boldsymbol{V}_G$. Collectively, we have matrices

$$\begin{aligned}\boldsymbol{V}_{G_\kappa} &= 1./(1./\boldsymbol{V}_{Q_G^\kappa} + 1./\boldsymbol{V}_{P_{H_\kappa}})\\ \hat{\boldsymbol{G}} &= \boldsymbol{V}_{G_\kappa}\cdot(\boldsymbol{Q}_{G_\kappa}./\boldsymbol{V}_{Q_G^\kappa} + \boldsymbol{P}_{H_\kappa}./\boldsymbol{V}_{P_{H_\kappa}}).\end{aligned}$$

B. UAMP for $f_{\boldsymbol{G}_\kappa}(\boldsymbol{G}_\kappa, \boldsymbol{H}_\kappa)$

As $\boldsymbol{G}_\kappa^{\mathrm{T}} = \boldsymbol{F}\boldsymbol{H}_\kappa^{\mathrm{T}}$, we can construct a pseudo-observation model of $\boldsymbol{H}_\kappa^{\mathrm{T}}$, i.e.,

$$\boldsymbol{Q}_{G_\kappa}^{\mathrm{T}} = \boldsymbol{F}\boldsymbol{H}_\kappa^{\mathrm{T}} + \boldsymbol{W}_{G_\kappa}, \tag{61}$$

where $\boldsymbol{W}_{G_\kappa} \in \mathbb{C}^{N\times P}$ denotes a white Gaussian noise matrix, and the variances of each element is given by the elements in $\boldsymbol{V}_{G_\kappa}^{\mathrm{T}}$. To use the UAMP algorithm, we transform (61) into

$$\boldsymbol{R}_{G_\kappa}^{\mathrm{T}} = \boldsymbol{U}_F^{\mathrm{H}}\boldsymbol{Q}_{G_\kappa}^{\mathrm{T}} = \boldsymbol{\Phi}_H\boldsymbol{H}_\kappa^{\mathrm{T}} + \boldsymbol{W}_{G_\kappa},$$

where $[\boldsymbol{U}_F, \Lambda_F, \boldsymbol{V}_F] = \text{SVD}(\boldsymbol{F})$, $\boldsymbol{R}_{G_\kappa}^{\text{T}} = \boldsymbol{U}_F^{\text{H}} \boldsymbol{Q}_{G_\kappa}^{\text{T}} \in \mathbb{C}^{P \times N}$ and $\boldsymbol{\Phi}_H = \Lambda_H \boldsymbol{V}_H \in \mathbb{C}^{P \times M}$. Then, according to UAMP, two auxiliary matrices $\boldsymbol{V}_{P_{H_\kappa}}$ and $\boldsymbol{P}_{H_\kappa}$ can be computed by

$$\boldsymbol{V}_{P_{H_\kappa}} = |\boldsymbol{\Phi}_H|^2 \boldsymbol{V}_{\boldsymbol{H}_\kappa}^{\text{T}}, \tag{62}$$

$$\boldsymbol{P}_{H_\kappa} = \boldsymbol{\Phi}_H \hat{\boldsymbol{H}}_\kappa^{\text{T}} - \boldsymbol{V}_{P_{H_\kappa}} \cdot \boldsymbol{S}_{H_\kappa}, \tag{63}$$

with which intermediate matrices $\boldsymbol{V}_{S_{H_\kappa}}$ and $\boldsymbol{S}_{H_\kappa}$ are updated as

$$\begin{aligned} \boldsymbol{V}_{S_{H_\kappa}} &= 1./(\boldsymbol{V}_{G_\kappa}^{\text{T}} + \boldsymbol{V}_{P_{H_\kappa}}), \\ \boldsymbol{S}_{H_\kappa} &= \boldsymbol{V}_{S_{H_\kappa}} \cdot (\boldsymbol{R}_{G_\kappa}^{\text{T}} - \boldsymbol{P}_{H_\kappa}). \end{aligned} \tag{64}$$

Then, we can compute matrices $\boldsymbol{Q}_{H_\kappa}$ and $\boldsymbol{V}_{\boldsymbol{Q}_{H_\kappa}}$ with

$$\boldsymbol{V}_{\boldsymbol{Q}_{H_\kappa}}^{\text{T}} = 1./(|\boldsymbol{\Phi}_{\boldsymbol{H}}^{\text{H}}|^2 \boldsymbol{V}_{S_{H_\kappa}}), \tag{65}$$

$$\boldsymbol{Q}_{H_\kappa}^{\text{T}} = \hat{\boldsymbol{H}}_\kappa^{\text{T}} + \boldsymbol{V}_{\boldsymbol{Q}_{H_\kappa}} \cdot (\boldsymbol{\Phi}_{\boldsymbol{H}}^{\text{H}} \boldsymbol{S}_{H_\kappa}). \tag{66}$$

The (n, m)-th elements of $\boldsymbol{V}_{\boldsymbol{Q}_{H_\kappa}}$ and $\boldsymbol{Q}_{H_\kappa}$ denoted as q_{mn}^κ and $\nu_{q_{mn}^\kappa}$ represent the mean and variance of extrinsic message $m_{h_{mn}^\kappa \to f_{h_{mn}^\kappa}}(h_{mn}^\kappa)$. Here message $m_{h_{mn}^\kappa \to f_{h_{mn}^\kappa}}(h_{mn}^\kappa)$ corresponded to the message (27) in the full digital case. So we can use (28)-(50) to get the belief $b(h_{mn}^\kappa) = \mathcal{CN}(h_{mn}^\kappa; \hat{h}_{mn}^\kappa, \nu_{h_{mn}^\kappa})$. Stacking $\hat{h}_{mn}^\kappa$ and $\nu_{h_{mn}^\kappa}, \forall m, n, \kappa$ into matrices $\hat{\boldsymbol{H}}, \boldsymbol{V}_H$ completes the message passing. The message passing procedure is summarized in Algorithm 2.

Algorithm 2 NNHMP Algorithm for Hybrid Receiver

Initialization: $\hat{\boldsymbol{H}}_\kappa = \boldsymbol{0}_{N \times M}$, $\boldsymbol{V}_{\boldsymbol{H}_\kappa} = \boldsymbol{1}_{N \times M}$, $\boldsymbol{S}_{H_\kappa} = \boldsymbol{0}_{P \times N}$, $\boldsymbol{V}_G = \boldsymbol{1}_{6N \times P}$, $\hat{\boldsymbol{G}} = \boldsymbol{0}_{6N \times P}$, $\hat{\boldsymbol{S}}_G = \boldsymbol{0}_{3L \times P}$, $\hat{\gamma} = 1$, $\kappa \in \{xx, xy, xz, yy, yz, zz\}$.

Repeat

1: $\boldsymbol{V}_{P_G} = |\boldsymbol{\Phi}|^{\cdot 2} \boldsymbol{V}_G$
2: $\boldsymbol{P}_G = \boldsymbol{\Phi} \hat{\boldsymbol{G}} - \boldsymbol{V}_{P_G} \cdot \hat{\boldsymbol{S}}_G$
3: $\boldsymbol{V}_{Z_G} = 1./(\hat{\gamma} + 1./\boldsymbol{V}_{P_G})$
4: $\boldsymbol{Z}_G = \boldsymbol{V}_{Z_G} \cdot (\hat{\gamma} \boldsymbol{R} + \boldsymbol{P}_G./\boldsymbol{V}_{P_G})$
5: Compute noise precision $\hat{\gamma}$ by (56)
6: $\boldsymbol{V}_{S_G} = 1./(\boldsymbol{V}_{P_G} + \hat{\gamma}^{-1})$
7: $\boldsymbol{S}_G = \boldsymbol{V}_{S_G} \cdot (\boldsymbol{R} - \hat{\boldsymbol{P}}_G)$
8: $\boldsymbol{V}_{Q_G} = 1./(|\boldsymbol{\Phi}^{\text{H}}|^{\cdot 2} \boldsymbol{V}_{S_G})$
9: $\boldsymbol{Q}_G = \hat{\boldsymbol{G}} + \boldsymbol{V}_{Q_G} \cdot (\boldsymbol{\Phi}^{\text{H}} \boldsymbol{S}_G)$
10: Obtain $\hat{g}_{mn}^\kappa$, and $\nu_{g_{mn}^\kappa}, \forall m, n, \kappa$ by (60), stack them into $\hat{\boldsymbol{G}}$ and $\boldsymbol{V}_G$
11: $\forall \kappa, \boldsymbol{R}_{G_\kappa}^{\text{T}} = \boldsymbol{U}_F^{\text{H}} \boldsymbol{Q}_{G_\kappa}^{\text{T}}$
12: $\forall \kappa, \boldsymbol{V}_{P_{H_\kappa}} = |\boldsymbol{\Phi}_H|^2 \boldsymbol{V}_{\boldsymbol{H}_\kappa}^{\text{T}}$
13: $\forall \kappa, \boldsymbol{P}_{H_\kappa} = \boldsymbol{\Phi}_H \hat{\boldsymbol{H}}_\kappa^{\text{T}} - \boldsymbol{V}_{P_{H_\kappa}} \cdot \boldsymbol{S}_{H_\kappa}$
14: $\forall \kappa, \boldsymbol{V}_{S_{H_\kappa}} = 1./(\boldsymbol{V}_{G_\kappa}^{\text{T}} + \boldsymbol{V}_{P_{H_\kappa}})$
15: $\forall \kappa, \boldsymbol{S}_{H_\kappa} = \boldsymbol{V}_{S_{H_\kappa}} \cdot (\boldsymbol{R}_{G_\kappa}^{\text{T}} - \boldsymbol{P}_{H_\kappa})$
16: $\forall \kappa, \boldsymbol{V}_{\boldsymbol{Q}_{H_\kappa}}^{\text{T}} = 1./(|\boldsymbol{\Phi}_{\boldsymbol{H}}^{\text{H}}|^2 \boldsymbol{V}_{S_{H_\kappa}})$
17: $\forall \kappa, \boldsymbol{Q}_{H_\kappa}^{\text{T}} = \hat{\boldsymbol{H}}_\kappa^{\text{T}} + \boldsymbol{V}_{\boldsymbol{Q}_{H_\kappa}} \cdot (\boldsymbol{\Phi}_{\boldsymbol{H}}^{\text{H}} \boldsymbol{S}_{H_\kappa})$
18: Obtain $\hat{\boldsymbol{H}}_\kappa, \boldsymbol{V}_{\boldsymbol{H}_\kappa}, \forall \kappa$ by lines $8-20$ of algorithm 1

Until terminated

VI. Simulation Results

In this section, we provide extensive numerical results to demonstrate the performance of the proposed method. The system settings are as follows. The carrier frequency is set to $f = 3$GHz, i.e., the wavelength $\lambda = 0.1m$. At the base station, we assume a surface with 10×10 antenna patches, i.e., $M = 100$. At the user side, the surface consists of 5×5 patches, i.e., $N = 25$. The patch sizes of the base station and the user are set to $\Delta_x^r = \Delta_y^r = 0.5\lambda$ and $\Delta_x^t = \Delta_y^t = 0.1\lambda$ respectively. Hence, the antenna aperture of the base station is $D = 0.5$m, leading to a Fraunhofer distance $2D^2/\lambda = 5$m. The modulation scheme used is QPSK, and the pilot QPSK symbols are randomly generated. We vary the number of received signal vectors L from 100 to 500. As mentioned before, the number of hidden nodes in the NN hidden layer $N_h = 50$. The coordinate of the first patch of the base station is $(x_1^r, y_1^r, z_1^r) = (0, 0, 0)$, and the coordinate of the first patch of the user is randomly generated with $x_1^t, y_1^t \sim \text{U}[-\lambda, \lambda]$, and $z_1^t \sim \text{U}[20\lambda, 40\lambda]$. We evaluate the performance of estimators in terms of the NMSE of the channel and the location of the user (if an estimator provides the estimate of the user location), i.e., NMSE_H and NMSE_p, which are defined as

$$\text{NMSE}_H = E\frac{\|\boldsymbol{H} - \hat{\boldsymbol{H}}\|^2}{\|\boldsymbol{H}\|^2}$$

$$\text{NMSE}_p = E\frac{\|[x_1^t, y_1^t, z_1^t]^T - [\hat{x}_1^t, \hat{y}_1^t, \hat{z}_1^t]^T\|^2}{\|[x_1^t, y_1^t, z_1^t]^T\|^2}$$

where (x_1^t, y_1^t, z_1^t) and $\boldsymbol{H}$ represent the user coordinate and the channel matrix, and $(\hat{x}_1^t, \hat{y}_1^t, \hat{z}_1^t)$ and $\hat{\boldsymbol{H}}$ denote their estimates.

To the best of our knowledge, there are no existing works on parametric HMIMO channel estimation in the literature. For comparison, we include the performance of the LS channel estimation based on (9), which is given as

$$\hat{\boldsymbol{H}}_{LS} = (\boldsymbol{S}^H \boldsymbol{S})^{-1} \boldsymbol{S}^H \boldsymbol{Y},$$

where the channel matrix is directly estimated, and the estimates of the user locations cannot be provided. It is also interesting to use the approximate channel model (11) for channel estimation. Noting that it is still complex, we can also develop an NN-assisted hybrid model to replace (11), then derive a message passing algorithm to achieve parametric channel estimation. As the channel model used is an approximate one, the related simulation results are indicated by "AppMod". We will show that the approximate model can lead to considerable performance loss due to its significant mismatch with the actual channel model. In addition, we also include two performance bounds. One bound is obtained by assuming the coordinate of the user, i.e., (x_1^t, y_1^t, z_1^t) is known, so that the channel matrix can be constructed using (15) (hence the bound will not change with SNR or the pilot length). Moreover, the CRLB of user location estimation is also included, and the derivation is shown in Appendix.

The NMSE performance of the estimators versus SNR with $L = 200$ and 500 are shown in Fig. 8, where (a) and (b) show NMSE_H and NMSE_p, respectively. It can be seen from Fig. 8 (a) that, with the increase of the SNR, the performance of the proposed method gradually approaches the bound with perfect user location. This is because the estimation accuracy of the user location is improved with the SNR as shown in Fig. 8 (b). As expected, the proposed method significantly outperforms the LS one due to the strategy of parametric estimation. We can see from Fig. 8 (b) that the performance of proposed method delivers performance close to the CRLB at low SNRs, while deviates from the CRLB at high SNRs due to the small model mismatch. In both Figs. 8 (a) and (b), we can also see that the proposed method delivers considerably better performance than

This article has been accepted for publication in IEEE Transactions on Wireless Communications. This is the author's version which has not been fully edited and content may change prior to final publication. Citation information: DOI 10.1109/TWC.2025.3552492

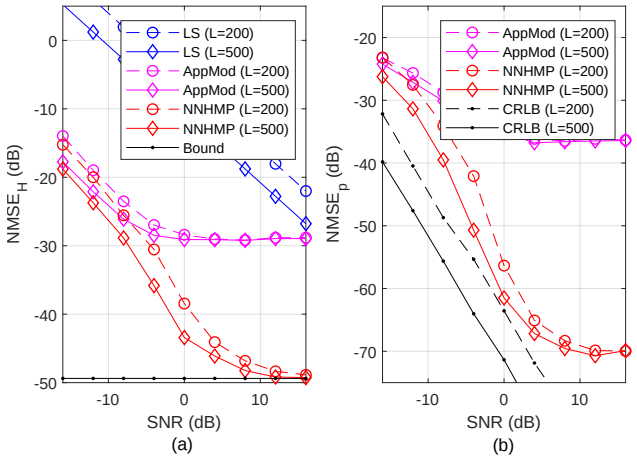

Fig. 8: NMSE performance of the estimators versus SNR.

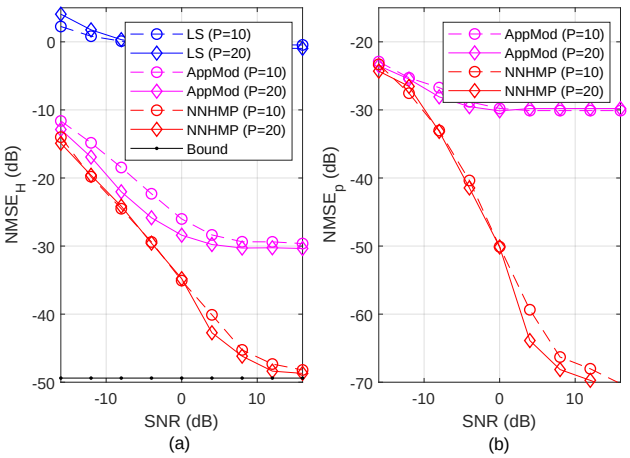

Fig. 11: NMSE of the estimators with hybrid receiver versus SNR.

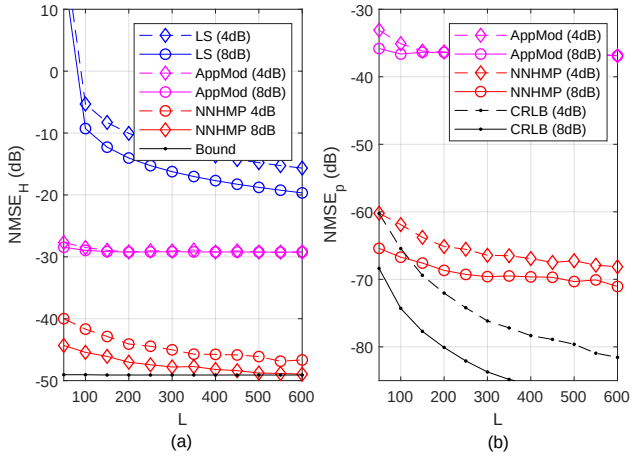

Fig. 9: NMSE performance of the estimators versus pilot length L .

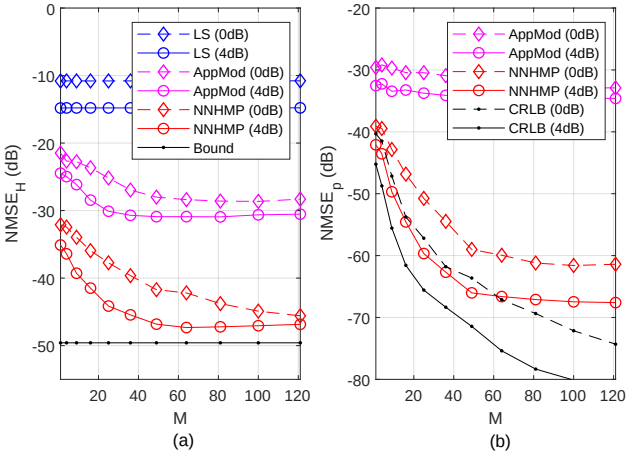

Fig. 10: NMSE performance of the estimators versus M.

AppMod, as the true channels can be well characterized by the proposed hybrid channel model. Due to the considerable model mismatch, AppMod exhibits a high error floor. For the proposed method, we observe a much lower error floor. This is because the NN with limited number of hidden nodes cannot perfectly model the channel.

Then we examine the performance of the methods versus the number of received signal vectors (i.e., the length of pilot signal) L in Fig. 9, where the SNR is set to 4dB and 8dB. As expected, with the increase of L, the performance of the LS and the proposed estimator improve. However, AppMod has a high error floor due to the significant model mismatch. We can see that the proposed estimator delivers significantly better performance and it approaches the performance bound when L is relatively large in Fig. 9(a). In Fig. 9(b), we can observe significant gaps between the performance of the proposed method and the CRLB. This is again because the small model mismatch of the proposed method dominates the error performance when the NMSE is very small (e.g., less than -70dB), resulting in an error floor.

In Fig. 10, we examine the estimation performance NMSE_H and NMSE_p versus the number of BS antenna patches M at various SNRs. With the increase of M, the NMSE performance of the parametric estimators improves until performance floors appear. Compared to AppMod, the proposed estimator has a much lower floor thanks to the high modeling capability of the hybrid channel model. We can also see that the performance of LS channel estimator does not improve. This is because the LS estimator is not a parametric one, and the number of channel coefficients to be estimated also increases with M. Again the gaps between the proposed method and CRLB is due to the small modelling error, which dominates the NMSE performance.

Next, we examine the performance of various estimators in the case of a hybrid receiver. The NMSE performance of the estimators versus SNR and the number of RF chains P is shown in Fig.11 and 12. From the results, it can be seen that with the increase of the number of RF chains and SNR, the performance of the estimators improves as expected. We again observe that AppMod has a high performance floor in all the cases due to the significant model mismatch and the LS estimator does not perform well as the dimension of the received signal vectors is significantly reduced. The proposed estimator achieves the best performance and performs significantly better than other estimators.

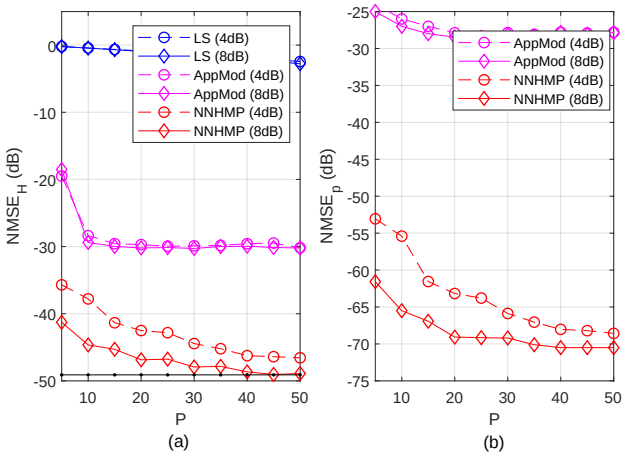

Fig. 12: NMSE of estimators with hybrid receiver versus P.

VII. Conclusions

In this paper, we have investigated the issue of channel estimation for HMIMO, where the channel is characterized by the dyadic Green's function. Considering that the channel matrix is parameterized with a few parameters, we propose a parametric channel estimation method to achieve superior estimation performance. To tackle the challenging complex nonlinear relationship between the parameters and channel coefficients, we develop a hybrid channel model with the aid of an NN. With the hybrid channel model, the estimation problem is formulated in a probabilistic form. Leveraging a factor graph representation and UAMP, an efficient message passing algorithm is developed. Extensive simulation results show the superior performance of the proposed method. Future work includes the extension of this work to the scenario with non-line-of-sight propagation, where a more challenging parameter estimation needs to be solved due to the presence of scatters.

Appendix A
Cramér-Rao Lower Bound Using the Hybrid Channel Model

It is worth mentioning that, regarding the user position estimation, the hybrid channel model provides a convenient way to obtain the CRLB thanks to its simpler expression.

According to (9), the received signal $\boldsymbol{Y} = (\boldsymbol{y}_m, ..., \boldsymbol{y}_M) \in \mathbb{C}^{3L\times M}$ is given as

$$\boldsymbol{Y} = \boldsymbol{S}\boldsymbol{H} + \boldsymbol{W},$$

where $\boldsymbol{W} \in \mathbb{C}^{3L\times M}$ is the AWGN with precision γ. We assume that the precision is known in the derivation of the CRLB, while it is estimated in the proposed method. Define vector $\boldsymbol{p} = [x_1^t, y_1^t, z_1^t]^T \in \mathbb{R}^{3\times 1}$, which includes the unknown coordinate. The logarithm of the likelihood function can be expressed as

$$\begin{aligned}\ln p(\boldsymbol{Y}|x_1^t, y_1^t, z_1^t) &= -\left\|\boldsymbol{Y} - \boldsymbol{S}\boldsymbol{H}\right\|^2 \gamma + C \\ &= -\sum_{m=1}^{M} \left\|\boldsymbol{y}_m - \boldsymbol{S}\boldsymbol{h}_m\right\|^2 \gamma + C\end{aligned}$$

where C is a constant, vectors $\boldsymbol{h}_m = [\boldsymbol{h}_{mn}^{\mathrm{T}}, ..., \boldsymbol{h}_{mN}^{\mathrm{T}}]^{\mathrm{T}}$, $\boldsymbol{h}_{mn} = [h_{mn}^{xx}, h_{mn}^{yy}, h_{mn}^{zz}, h_{mn}^{xy}, h_{mn}^{xz}, h_{mn}^{yz}]^{\mathrm{T}} \in \mathbb{C}^{6\times 1}$. Then, we define $f(\boldsymbol{p}) = \sum_{m=1}^{M} f_m(\boldsymbol{p})$, where $f_m(\boldsymbol{p}) = -\left\|\boldsymbol{y}_m - \boldsymbol{S}\boldsymbol{h}_m\right\|^2 \gamma$.

The Fisher information matrix (FIM) $\boldsymbol{\mathcal{F}}(\boldsymbol{p}) \in \mathbb{R}^{3\times 3}$ can be obtained as

$$\boldsymbol{\mathcal{F}}(\boldsymbol{p}) = -\mathbb{E}\begin{bmatrix} \frac{\partial^2 f(\boldsymbol{p})}{\partial x_1^t \partial x_1^t} & \frac{\partial^2 f(\boldsymbol{p})}{\partial x_1^t \partial y} & \frac{\partial^2 f(\boldsymbol{p})}{\partial x_1^t \partial z_1^t} \\ \frac{\partial^2 f(\boldsymbol{p})}{\partial y \partial x_1^t} & \frac{\partial^2 f(\boldsymbol{p})}{\partial y \partial y} & \frac{\partial^2 f(\boldsymbol{p})}{\partial y \partial z_1^t} \\ \frac{\partial^2 f(\boldsymbol{p})}{\partial z_1^t \partial x_1^t} & \frac{\partial^2 f(\boldsymbol{p})}{\partial z_1^t \partial y} & \frac{\partial^2 f(\boldsymbol{p})}{\partial z_1^t \partial z_1^t} \end{bmatrix}.$$

In the following, we only take element $\frac{\partial^2 f(\boldsymbol{p})}{\partial x_1^t \partial y_1^t}$ as example, and derivations for other elements will be the same. We have

$$\frac{\partial^2 f(\boldsymbol{p})}{\partial x_1^t \partial y_1^t} = \sum_m \frac{\partial^2 f_m(\boldsymbol{p})}{\partial x_1^t \partial y_1^t}$$

where

$$\begin{aligned}\frac{\partial^2 f_m(\boldsymbol{p})}{\partial x_1^t \partial y_1^t} = \gamma\Big(&\boldsymbol{y}_m^H \boldsymbol{S} \frac{\partial^2 \boldsymbol{h}_m}{\partial x_1^t \partial y_1^t} + \frac{\partial^2 \boldsymbol{h}_m^H}{\partial x_1^t \partial y_1^t} \boldsymbol{S}^H \boldsymbol{y} - \frac{\partial^2 \boldsymbol{h}_m^H}{\partial x_1^t \partial y_1^t} \boldsymbol{S}^H \boldsymbol{S} \boldsymbol{h}_m \\ &- \frac{\partial \boldsymbol{h}_m^H}{\partial x_1^t} \boldsymbol{S}^H \boldsymbol{S} \frac{\partial \boldsymbol{h}_m}{\partial y_1^t} - \frac{\partial \boldsymbol{h}_m^H}{\partial y_1^t} \boldsymbol{S}^H \boldsymbol{S} \frac{\partial \boldsymbol{h}_m}{\partial x_1^t} - \boldsymbol{h}_m^H \boldsymbol{S}^H \boldsymbol{S} \frac{\partial^2 \boldsymbol{h}_m}{\partial x_1^t \partial y_1^t}\Big),\end{aligned}$$

The partial derivation $\frac{\partial \boldsymbol{h}_{mn}}{\partial x_1^t} = \left(\frac{\partial h_{mn}^{xx}}{\partial x_1^t}, ..., \frac{\partial h_{mn}^{yz}}{\partial x_1^t}\right)$ and $\frac{\partial^2 \boldsymbol{h}_m}{\partial x_1^t \partial y_1^t} = \left(\frac{\partial^2 h_m^{xx}}{\partial x_1^t \partial y_1^t}, ..., \frac{\partial^2 h_{mn}^{yz}}{\partial x_1^t \partial y_1^t}\right)$. From (15) we have $h_{mn}^{\kappa} = \varphi^{\kappa}(x_{mn}, y_{mn}, z_{mn}) \exp(ik_0 r_{mn}), \forall \kappa \in \{xx, ..., yz\}$, with

$$\begin{aligned}\phi_{mn}^{\kappa} &\triangleq \varphi^{\kappa}(x_{mn}, y_{mn}, z_{mn}) \\ &= \varphi^{\kappa}(x_1^t + \Delta_{mn}^x, y_1^t + \Delta_{mn}^y, z_1^t)\end{aligned}$$

where Δ_{mn}^x and Δ_{mn}^y are defined in (16), representing the offset of (m,n)-th patch pair in the x, y directions, respectively. So the first and second partial derivatives are obtained as

$$\frac{\partial h_{mn}^{\kappa}}{\partial x_1^t} = \left(\frac{\partial \phi_{mn}^{\kappa}}{\partial x_1^t} + ik_0 \phi_{mn}^{\kappa} \frac{\partial r_{mn}}{\partial x_1^t}\right) \exp(ik_0 r_{mn}).$$

$$\begin{aligned}&\frac{\partial h_{mn}^{\kappa}}{\partial x_1^t \partial y_1^t} = \\ &\frac{\partial}{\partial y_1^t}\left(\frac{\partial \phi_{mn}^{\kappa}}{\partial x_1^t} \exp(ik_0 r_{mn}) + ik_0 \phi_{mn}^{\kappa} \frac{\partial r_{mn}}{\partial x_1^t} \exp(ik_0 r_{mn})\right) \\ &= \Bigg(\frac{\partial^2 \phi_{mn}^{\kappa}}{\partial x_1^t \partial y_1^t} + ik_0 \Bigg(\frac{\partial \phi_{mn}^{\kappa}}{\partial x_1^t} \frac{\partial r_{mn}}{\partial y_1^t} + \frac{\partial \phi_{mn}^{\kappa}}{\partial y_1^t} \frac{\partial r_{mn}}{\partial x_1^t} \\ &\quad + \phi_{mn}^{\kappa} \frac{\partial^2 r_{mn}}{\partial x_1^t \partial y_1^t} + ik_0 \phi_{mn}^{\kappa} \frac{\partial r_{mn}}{\partial x_1^t} \frac{\partial r_{mn}}{\partial y_1^t}\Bigg)\Bigg) \exp(ik_0 r_{mn}).\end{aligned}$$

As $\phi_{mn}^{\kappa} = (\boldsymbol{w}_{2,\kappa_1} + \boldsymbol{w}_{2,\kappa_1})^{\mathrm{T}} g_a(x_{mn}\boldsymbol{w}_1^x + y_{mn}\boldsymbol{w}_1^y + z_{mn}\boldsymbol{w}_1^z + \boldsymbol{b}_1)$, the first and second order partial derivatives of ϕ_{mn}^{κ} are given as

$$\begin{aligned}\frac{\partial \phi_{mn}^{\kappa}}{\partial x_1^t} &= \left((\boldsymbol{w}_{2,\kappa_1} + \boldsymbol{w}_{2,\kappa_1}) \cdot \boldsymbol{w}_1^x\right)^{\mathrm{T}} g_a'(\boldsymbol{c}_{mn}), \\ \frac{\partial^2 \phi_{mn}^{\kappa}}{\partial x_1^t \partial y_1^t} &= \left((\boldsymbol{w}_{2,1} + \boldsymbol{w}_{2,7}) \cdot (\boldsymbol{w}_1^x \cdot \boldsymbol{w}_1^y)\right)^T g_a''(\boldsymbol{c}_{mn}),\end{aligned}$$

where $\boldsymbol{c}_{mn} = x_{mn}\boldsymbol{w}_1^x + y_{mn}\boldsymbol{w}_1^y + z_{mn}\boldsymbol{w}_1^z + \boldsymbol{b}_1$, and indices κ_1 and κ_2 depend on κ. The first and second derivatives of $g_a(\cdot)$ are

$$g_a'(\cdot) = 1 - g_a^2(\cdot), \quad g_a''(\cdot) = 2g_a(\cdot)\left(g_a^2(\cdot) - 1\right).$$

The CRLB of $\boldsymbol{p}$ is given as $\mathrm{CRLB}_{\boldsymbol{p}} = \mathrm{Trace}(\boldsymbol{\mathcal{F}}^{-1}(\boldsymbol{p}))$.

REFERENCES

[1] J. An, C. Yuen, C. Huang, M. Debbah, H. Vincent Poor, and L. Hanzo, "A tutorial on holographic MIMO communications—part I: Channel modeling and channel estimation," *IEEE Communications Letters*, vol. 27, no. 7, pp. 1664–1668, 2023.

[2] J. An, C. Yuen, C. Huang, M. Debbah, H. V. Poor, and L. Hanzo, "A tutorial on holographic MIMO communications—part II: Performance analysis and holographic beamforming," *IEEE Communications Letters*, vol. 27, no. 7, pp. 1669–1673, 2023.

[3] L. Wei, C. Huang, G. C. Alexandropoulos, W. E. I. Sha, Z. Zhang, M. Debbah, and C. Yuen, "Multi-user holographic MIMO surfaces: Channel modeling and spectral efficiency analysis," *IEEE Journal of Selected Topics in Signal Processing*, vol. 16, no. 5, pp. 1112–1124, 2022.

[4] L. Wei, C. Huang, G. C. Alexandropoulos, Z. Yang, J. Yang, W. E. I. Sha, Z. Zhang, M. Debbah, and C. Yuen, "Tri-polarized holographic MIMO surfaces for near-field communications: Channel modeling and precoding design," *IEEE Transactions on Wireless Communications*, vol. 22, no. 12, pp. 8828–8842, 2023.

[5] A. Adhikary, M. S. Munir, A. D. Raha, Y. Qiao, Z. Han, and C. S. Hong, "Integrated sensing, localization, and communication in holographic MIMO-enabled wireless network: A deep learning approach," *IEEE Transactions on Network and Service Management*, vol. 21, no. 1, pp. 789–809, 2024.

[6] C. Huang, S. Hu, G. C. Alexandropoulos, A. Zappone, C. Yuen, R. Zhang, M. D. Renzo, and M. Debbah, "Holographic MIMO surfaces for 6G wireless networks: Opportunities, challenges, and trends," *IEEE Wireless Communications*, vol. 27, no. 5, pp. 118–125, 2020.

[7] L. Sanguinetti, A. A. D'Amico, and M. Debbah, "Wavenumber-division multiplexing in line-of-sight holographic MIMO communications," *IEEE Transactions on Wireless Communications*, vol. 22, no. 4, pp. 2186–2201, 2023.

[8] R. Deng, B. Di, H. Zhang, Y. Tan, and L. Song, "Reconfigurable holographic surface: Holographic beamforming for metasurface-aided wireless communications," *IEEE Transactions on Vehicular Technology*, vol. 70, no. 6, pp. 6255–6259, 2021.

[9] A. A. D'Amico, A. d. J. Torres, L. Sanguinetti, and M. Win, "Cramér-rao bounds for holographic positioning," *IEEE Transactions on Signal Processing*, vol. 70, pp. 5518–5532, 2022.

[10] R. Deng, B. Di, H. Zhang, H. V. Poor, and L. Song, "Holographic MIMO for LEO satellite communications aided by reconfigurable holographic surfaces," *IEEE Journal on Selected Areas in Communications*, vol. 40, no. 10, pp. 3071–3085, 2022.

[11] H. Zhang, H. Zhang, B. Di, M. D. Renzo, Z. Han, H. V. Poor, and L. Song, "Holographic integrated sensing and communication," *IEEE Journal on Selected Areas in Communications*, vol. 40, no. 7, pp. 2114–2130, 2022.

[12] Ö. T. Demir, E. Björnson, and L. Sanguinetti, "Channel modeling and channel estimation for holographic massive MIMO with planar arrays," *IEEE Wireless Communications Letters*, vol. 11, no. 5, pp. 997–1001, 2022.

[13] A. A. D'Amico, G. Bacci, and L. Sanguinetti, "DFT-based channel estimation for holographic MIMO," *arXiv preprint arXiv:2306.05156*, 2023.

[14] W. Yu, H. He, X. Yu, S. Song, J. Zhang, r. D. Murch, and K. B. Letaief, "Learning bayes-optimal channel estimation for holographic MIMO in unknown EM environments," *arXiv preprint arXiv:2311.07908*, 2023.

[15] Y. Chen, Y. Wang, Z. Wang, and Z. Han, "Angular-distance based channel estimation for holographic MIMO," *arXiv preprint arXiv:2311.15158*, 2023.

[16] M. Ghermezcheshmeh and N. Zlatanov, "Parametric channel estimation for LoS dominated holographic massive MIMO systems," *IEEE Access*, vol. 11, pp. 44 711–44 724, 2023.

[17] S. S. A. Yuan, Z. He, X. Chen, C. Huang, and W. E. I. Sha, "Electromagnetic effective degree of freedom of an MIMO system in free space," *IEEE Antennas and Wireless Propagation Letters*, vol. 21, no. 3, pp. 446–450, 2022.

[18] S. S. A. Yuan and W. E. I. Sha, "Electromagnetic degree of freedom of a MIMO communication system," in *2022 IEEE 5th International Conference on Electronic Information and Communication Technology (ICEICT)*, 2022, pp. 667–669.

[19] W. Yu, H. He, X. Yu, S. Song, J. Zhang, R. D. Murch, and K. B. Letaief, "Bayes-optimal unsupervised learning for channel estimation in near-field holographic MIMO," *arXiv preprint arXiv:2312.10438*, 2023.

[20] Y. Shi, L. Lian, Y. Shi, Z. Wang, Y. Zhou, L. Fu, L. Bai, J. Zhang, and W. Zhang, "Machine learning for large-scale optimization in 6g wireless networks," *IEEE Communications Surveys Tutorials*, vol. 25, no. 4, pp. 2088–2132, 2023.

[21] W. Yu, Y. Ma, H. He, S. Song, J. Zhang, and K. B. Letaief, "Deep learning for near-field xl-mimo transceiver design: Principles and techniques," *arXiv preprint arXiv:2309.09575*, 2024.

[22] Y. Chen, X. Guo, Z. Wang, and C. Yuen, "Unifying far-field and near-field wireless communications in 6g mimo," *IEEE Wireless Communications Letters*, vol. 13, no. 10, pp. 2762–2766, 2024.

[23] Y. Chen, X. Guo, G. Zhou, S. Jin, D. K. Ng, and Z. Wang, "Unified far-field and near-field in holographic mimo: A wavenumber-domain perspective," *arXiv preprint arXiv:2407.14815*, 2024.

[24] S. Guo, J. Ye, K. Qu, and S. Dang, "Green holographic MIMO communications with a few transmit radio frequency chains," *IEEE Transactions on Green Communications and Networking*, vol. 8, no. 1, pp. 90–102, 2024.

[25] Q. Guo and J. Xi, "Approximate message passing with unitary transformation," *arXiv preprint arXiv:1504.04799*, 2015.

[26] Z. Yuan, Q. Guo, and M. Luo, "Approximate message passing with unitary transformation for robust bilinear recovery," *IEEE Transactions on Signal Processing*, vol. 69, pp. 617–630, 2020.

[27] M. Luo, Q. Guo, M. Jin, Y. C. Eldar, D. Huang, and X. Meng, "Unitary approximate message passing for sparse bayesian learning," *IEEE Transactions on Signal Processing*, vol. 69, pp. 6023–6039, 2021.

[28] S. M. Mikki and Y. M. M. Antar, "A theory of antenna electromagnetic near field—part II," *IEEE Transactions on Antennas and Propagation*, vol. 59, no. 12, pp. 4706–4724, 2011.

[29] H. F. Arnoldus, "Representation of the near-field, middle-field, and far-field electromagnetic Green's functions in reciprocal space," *JOSA B*, vol. 18, no. 4, pp. 547–555, 2001.

[30] S. M. Mikki, S. Clauzier, and Y. M. M. Antar, "Empirical geometrical bounds on MIMO antenna arrays for optimum diversity gain performance: An electromagnetic design approach," *IEEE Access*, vol. 6, pp. 39 876–39 894, 2018.

[31] J. Zhang, X. Yu, and K. B. Letaief, "Hybrid beamforming for 5G and beyond millimeter-wave systems: A holistic view," *IEEE Open Journal of the Communications Society*, vol. 1, pp. 77–91, 2019.

Zhengdao Yuan received the B.E. degree in communication and information system from the Henan University of Science and Technology in 2006, and the M. E. degree in communication engineering from Soochow University in 2009, and the Ph.D. degree in information and communication engineering from the National Digital Switching System Engineering and Technological Research Center in 2018. He is currently an Associate Professor with the Open University of Henan. He was a visiting scholar with the University of Wollongong in 2019. His research interests are mainly in massive MIMO, sparse channel estimation, message passing algorithm, and iterative receiver.

Yabo Guo received the B.E. degree in communication engineering from the North China University of Water Resources and Electric Power, Zhengzhou, China, in 2017, and the Ph.D. degree from Zhengzhou University, Zhengzhou, in 2024. He was a visiting Ph.D. student with the School of Electrical, Computer and Telecommunications Engineering, University of Wollongong, Wollongong, NSW, Australia, in 2024. His research interests are reconfigurable intelligent surface, holographic communication, message passing algorithm, and channel estimation.

Dawei Gao received the B. E. and Ph. D. degrees in telecommunications engineering from the University of Wollongong, Wollongong, NSW, Australia in 2016 and 2020, respectively. He is currently a Lecturer with the Hangzhou Institute of Technology, Xidian University, Hangzhou, Zhejiang, China. His research interests include machine learning, array signal processing and joint sensing and communications.

Qinghua Guo (S'07-M'08-SM'18) received the B.E. degree in electronic engineering and the M.E. degree in signal and information processing from Xidian University, in 2001 and 2004, respectively, and the Ph.D. degree in electronic engineering from the City University of Hong Kong in 2008. He is currently an Associate Professor with the School of Electrical, Computer and Telecommunications Engineering, University of Wollongong, Wollongong, NSW, Australia, and an Adjunct Associate Professor with the School of Engineering, The University of Western Australia, Perth, WA, Australia. His research interests include signal processing, Bayesian inference, machine learning for signal processing, communications, radar, and optical sensing. He was a recipient of the Australian Research Council's inaugural Discovery Early Career Researcher Award in 2012. Dr. Guo serves as an Associate Editor for IEEE Transactions on Signal Processing and IEEE Wireless Communications Letters.

Zhongyong Wang received the B.S. and M.S. degrees in automatic control from Harbin Shipbuilding Engineering Institute, Harbin, China, in 1986 and 1988, respectively, and the Ph.D. degree in automatic control theory and application from Xian Jiaotong University, Xi'an, China, in 1998. Since 1988, He has been with the Department of Electronics, Zhengzhou University, Zhengzhou, China, as a Lecturer. From 1999 to 2002, he was an Associate Professor, in 2002, and he was promoted to Professor with the Department of Communication Engineering. His research interests include numerous aspects within embedded systems, signal processing, and communication theory.

Chongwen Huang obtained his B. Sc. degree in 2010 from Nankai University, and the M.Sc degree from the University of Electronic Science and Technology of China in 2013, and PhD degree from Singapore University of Technology and Design (SUTD) in 2019. From Oct. 2019 to Sep. 2020, he is a Postdoc in SUTD. Since Sep. 2020, he joined into Zhejiang University as a tenure-track young professor. Dr. Huang is the recipient of 2021 IEEE Marconi Prize Paper Award, 2023 IEEE Fred W. Ellersick Prize Paper Award and 2021 IEEE ComSoc Asia-Pacific Outstanding Young Researcher Award. He has served as an Editor of IEEE Communications Letter, Elsevier Signal Processing, EURASIP Journal on Wireless Communications and Networking and Physical Communication since 2021. His main research interests are focused on Holographic MIMO Surface/Reconfigurable Intelligent Surface, B5G/6G Wireless Communications, mmWave/THz Communications, Deep Learning technologies for Wireless communications, etc.

Ming Jin (M'12-SM'24) received the B.E. degree in electronic engineering and the M.E. degree in signal and information processing from Xidian University, Xi'an, China, in 2005 and 2010, respectively. From 2013 to 2014, he was an Associate Researcher with the School of Electrical, Computer and Telecommunications Engineering, University of Wollongong, Wollongong, NSW, Australia. He is currently a Professor with the Faculty of Electrical Engineering and Computer Science, Ningbo University, Ningbo, China. His research interests include cognitive radio, localization, DOA estimation and UAV detection.

K ai-Kit Wong (M'01-SM'08-F'16) received the BEng, the MPhil, and the PhD degrees, all in Electrical and Electronic Engineering, from the Hong Kong University of Science and Technology, Hong Kong, in 1996, 1998, and 2001, respectively. After graduation, he took up academic and research positions at the University of Hong Kong, Lucent Technologies, Bell-Labs, Holmdel, the Smart Antennas Research Group of Stanford University, and the University of Hull, UK. He is Chair in Wireless Communications at the Department of Electronic and Electrical Engineering, University College London, UK. His current research centers around 6G and beyond mobile communications. He is Fellow of IEEE and IET. He served as the Editor-in-Chief for IEEE Wireless Communications Letters between 2020 and 2023.